Am J Physiol Renal Physiol 318: F117–F134, 2020.
First published November 18, 2019; doi:10.1152/ajprenal.00108.2019.

RESEARCH ARTICLE | *Mechanism and Treatment of Renal Fibrosis*

Inhibition of tyrosine kinase receptor signaling attenuates fibrogenesis in an ex vivo model of human renal fibrosis

Emilia Bigaeva,[1]* Elisabeth G. D. Stribos,[1,2]* Henricus A. M. Mutsaers,[1,3] Bram Piersma,[6] Anna M. Leliveld,[5] Igle J. de Jong,[5] Ruud A. Bank,[6] Marc A. Seelen,[2] Harry van Goor,[6] Lutz Wollin,[4] Peter Olinga,[1] and Miriam Boersema[1]

[1]*Department of Pharmaceutical Technology and Biopharmacy, Groningen Research Institute of Pharmacy, University of Groningen, Groningen, The Netherlands;* [2]*Division of Nephrology, Department of Internal Medicine, University Medical Center University of Groningen, Groningen, The Netherlands;* [3]*Department of Clinical Medicine, Aarhus University, Aarhus, Denmark;* [4]*Boehringer Ingelheim Pharma, Biberach, Germany;* [5]*Department of Urology, University Medical Center Groningen, University of Groningen, Groningen, The Netherlands; and* [6]*Department of Pathology and Medical Biology, University Medical Center Groningen, University of Groningen, Groningen, The Netherlands*

Submitted 8 March 2019; accepted in final form 5 November 2019

Bigaeva E, Stribos EG, Mutsaers HA, Piersma B, Leliveld AM, de Jong IJ, Bank RA, Seelen MA, van Goor H, Wollin L, Olinga P, Boersema M. Inhibition of tyrosine kinase receptor signaling attenuates fibrogenesis in an ex vivo model of human renal fibrosis. *Am J Physiol Renal Physiol* 318: F117–F134, 2020. First published November 18, 2019; doi:10.1152/ajprenal.00108.2019.—Poor translation from animal studies to human clinical trials is one of the main hurdles in the development of new drugs. Here, we used precision-cut kidney slices (PCKS) as a translational model to study renal fibrosis and to investigate whether inhibition of tyrosine kinase receptors, with the selective inhibitor nintedanib, can halt fibrosis in murine and human PCKS. We used renal tissue of murine and human origins to obtain PCKS. Control slices and slices treated with nintedanib were studied to assess viability, activation of tyrosine kinase receptors, cell proliferation, collagen type I accumulation, and gene and protein regulation. During culture, PCKS spontaneously develop a fibrotic response that resembles in vivo fibrogenesis. Nintedanib blocked culture-induced phosphorylation of platelet-derived growth factor receptor and vascular endothelial growth factor receptor. Furthermore, nintedanib inhibited cell proliferation and reduced collagen type I accumulation and expression of fibrosis-related genes in healthy murine and human PCKS. Modulation of extracellular matrix homeostasis was achieved already at 0.1 μM, whereas high concentrations (1 and 5 μM) elicited possible nonselective effects. In PCKS from human diseased renal tissue, nintedanib showed limited capacity to reverse established fibrosis. In conclusion, nintedanib attenuated the onset of fibrosis in both murine and human PCKS by inhibiting the phosphorylation of tyrosine kinase receptors; however, the reversal of established fibrosis was not achieved.

nintedanib; precision-cut kidney slices; renal fibrosis; tyrosine kinase receptor

INTRODUCTION

Renal fibrosis, defined by the progressive deposition of connective tissue, is a hallmark of chronic kidney disease (CKD), which affects an estimated 10% of the population in developed countries (19). CKD progresses to end-stage renal disease, which eventually requires replacement therapy (dialysis or transplantation). Current research investigates strategies to halt CKD progression or even to reverse renal fibrosis (6, 37). However, no effective therapy has been clinically implemented.

Pathological activation of various receptor tyrosine kinases (RTKs), such as platelet-derived growth factor (PDGF), fibroblast growth factor (FGF), and epidermal growth factor (EGF) receptors, plays a key role in renal fibrogenesis (3, 5, 29, 36, 44). The PDGF receptor (PDGFR) is an attractive molecular target for antifibrotic therapies (37a) since PDGFR signaling is involved in the transdifferentiation of collagen-producing myofibroblasts (7, 9, 18). PDGFRα and PDGFRβ are expressed in renal tissue mainly by glomerular mesangial cells, interstitial fibroblasts, and vascular smooth muscle cells (4). Several studies have reported an increased expression of both receptors in murine and human renal disease (7, 12). Activation of PDGFR leads to glomerulosclerosis and (tubulo)interstitial fibrosis (29). Therefore, blocking PDGFR signaling is a promising strategy to halt the progression of renal fibrosis.

Nintedanib is a small-molecule tyrosine kinase inhibitor approved in several countries worldwide for the treatment of idiopathic pulmonary fibrosis and for the second-line treatment of non-small-cell lung carcinoma with adenocarcinoma histology. Nintedanib affects signaling pathways of multiple growth factors, including VEGF, FGF, and PDGF, as well as lymphocyte-specific protein tyrosine kinase and Src nonreceptor kinases (32, 41). In a phase II randomized clinical trial, nintedanib showed antiangiogenic effects and had an acceptable safety profile in patients with advanced renal cell carcinoma (10). To our knowledge, the impact of nintedanib on human renal fibrosis has not been published.

The lack of translational models of human renal fibrosis hampers the search for effective antifibrotic therapies (33). In vitro models lack cellular heterogeneity, and animal models have limited implications for human disease. To partly overcome these limitations, we used precision-cut

* E. Bigaeva and E. G. D. Stribos contributed equally to this work.

Address for reprint requests and other correspondence: P. Olinga, Dept. of Pharmaceutical Technology and Biopharmacy, Univ. of Groningen, Antonius Deusinglaan 1, Groningen 9713 AV, The Netherlands (e-mail: p.olinga@rug.nl).

Table 1. *Patient demographics*

	Healthy Renal Tissue	Fibrotic Renal Tissue
n	9	10
Sex, % male/femle	67/33	40/60
Age, yr	66 ± 8	47 ± 15
Nephrectomy side, % left	37.5	50
Creatinine before nephrectomy, μmol/L	81 ± 13	545 ± 403
Estimated glomerular filtration rate before nephrectomy, mL·min^{-1}·1.73 m^{-2}*	81 ± 9	NA
Time on dialysis (mean), mo	NA	116 ± 136
Time since (first) transplantation (mean), mo	NA	132 ± 150
Type of renal tissue	NA	Nonfunctioning kidney allograft (n = 4), kidney allograft with infected abscess (n = 1), nonfunctioning native kidney with end-stage renal disease (n = 5)

Values are presented as means ± SD unless otherwise indicated. NA, not applicable. *Calculated using the Modification of Diet in Renal Disease formula.

kidney slices (PCKS) as an ex vivo model of renal fibrosis (13, 34, 43). PCKS replicate the organotypic multicellular characteristics, as one slice maintains the complex three-dimensional architecture of the kidney, and have a high translational impact, as both murine and human tissue, healthy and diseased, can be used. In addition, PCKS culture is reproducible and allows for a substantial reduction of animal use, making it a promising preclinical tool for drug development.

In the present study, we aimed to investigate the therapeutic effects of nintedanib in PCKS and to find whether inhibition of nintedanib's molecular targets may prevent renal fibrosis in murine and, more importantly, human kidneys.

MATERIALS AND METHODS

Ethics Statement

This study was approved by the Medical Ethical Committee of the University Medical Center Groningen according to Dutch legislation and the Code of Conduct for dealing responsibly with human tissue in the context of health research (https://www.federa.org/), forgoing the need of written consent for "further use" of coded, anonymous human tissue.

The animal experiments were approved by the Animal Ethics Committee of the University of Groningen (DEC 6416AA-001).

Renal Tissue

Macroscopically healthy renal cortical tissue (n = 9) was obtained from tumor nephrectomies, and fibrotic renal tissue (n = 10) was obtained from end-stage renal disease nephrectomies or transplantectomies. Table 1 shows patient demographics. Renal tissue was stored in ice-cold University of Wisconsin organ preservation solution, and the cold ischemia time was limited to 2–3 h.

Murine tissue was obtained from male C57BL/6 mice with an average weight of 28.3 ± 2.4 g and 12.1 ± 2.2 wk of age. Animals were housed in filter-top cages with free access to water and food. Kidneys were harvested via a terminal procedure, performed under isoflurane/O_2 anesthesia (Pharmachemie, Haarlem, The Netherlands), and stored in ice-cold University of Wisconsin solution until further use.

Preparation and Treatment of PCKS

PCKS were prepared according to the protocol by Poosti et al. (30) (mouse) and Stribos et al. (34) (human) using a Krumdieck tissue slicer. Slices were incubated in Williams' medium E with GlutaMAX (Life Technologies, Carlsbad, CA) containing 10 μg/mL ciprofloxacin and 26 mM glucose at 37°C in an 80% O_2-5% CO_2 atmosphere while gently shaken. Culture medium was used without serum supplementation to avoid the associated batch-to-batch variability (i.e., to establish fully controlled environment). Nintedanib was kindly provided by Boehringer Ingelheim (Biberach, Germany). We treated murine and human PCKS with nintedanib (0.1–10 μM) for 48 h. Analyses were performed using three pooled slices from the same animal/donor (technical replicates) from at least three to five animals or donors (biological replicates).

Viability of PCKS

Viability of the slices was assessed by measuring ATP content using the ATP bioluminescence kit (Roche Diagnostics, Mannheim, Germany), as previously described in Ref. 39.

Quantitative Real-Time PCR and Low-Density Array

Total RNA was extracted with the RNeasy mini kit (Qiagen, Venlo, The Netherlands) and reverse transcribed using the Reverse Transcription System (Promega, Leiden, The Netherlands). cDNA was used for quantitative real-time PCR performed with a Viia7 Real-Time PCR system (Applied Biosystems, Bleiswijk, The Netherlands). Gene expression was calculated using the $2^{-\Delta C_t}$ method (where C_t is threshold cycle) (26) and corrected for *GAPDH*. The Taqman gene expression assays used in this study are described in Supplemental Table S1 (all Supplemental Data for this article are available online at https://doi.org/10.6084/m9.figshare.9999557.v1).

Fig. 1. *A*: schematic illustration of the workflow. Renal tissue of murine or human origin was used to obtain cylindrical cores. By placing the tissue cores in a Krumdieck tissue slicer filled with ice-cold Krebs-Henseleit buffer, we prepared precision-cut kidney slices (PCKS) with a wet weight of 4–5 mg and estimated thickness of 250–300 μm. Slices were subsequently incubated in 12-well plates (1 slice/well) in culture medium with or without nintedanib for 48 h at 37°C. Medium was refreshed at 24 h. At the end of culture period, samples were collected by pooling three slices from each animal/donor for each type of analysis. Visualization of kidney slices prepared from healthy tissue is represented by the blue color, and diseased tissue is represented by the orange color. *B*: viability of murine PCKS (mPCKS), human PCKS (hPCKS), and fibrotic human PCKS (fhPCKS) treated with nintedanib for 48 h was measured by ATP and total protein content. Data are shown as values relative to nontreated control slices at 48 h and are expressed as means ± SE; n = 4–5. *$P < 0.05$. *C*: representative images of periodic acid-Schiff staining of untreated slices at 0 h and 48 h as well as of slices treated with 5 μM nintedanib (scale bar = 100 μm).

The expression of 44 genes related to fibrosis (Supplemental Table S2) was examined using a custom-designed low-density array (Applied Biosystems) (31). cDNA from renal tissue of C57BL/6 control mice that underwent unilateral ureteral obstruction (UUO) microsurgery was kindly provided by Dr. Bram Piersma. A total of 100 μL of reaction mixture containing 6 ng/μL cDNA and 50 μL 2× Taqman Universal PCR Master Mix (Applied Biosystems) was loaded per sample. PCR amplification was performed on a Viia7 Real-Time PCR system (Applied Biosystems).

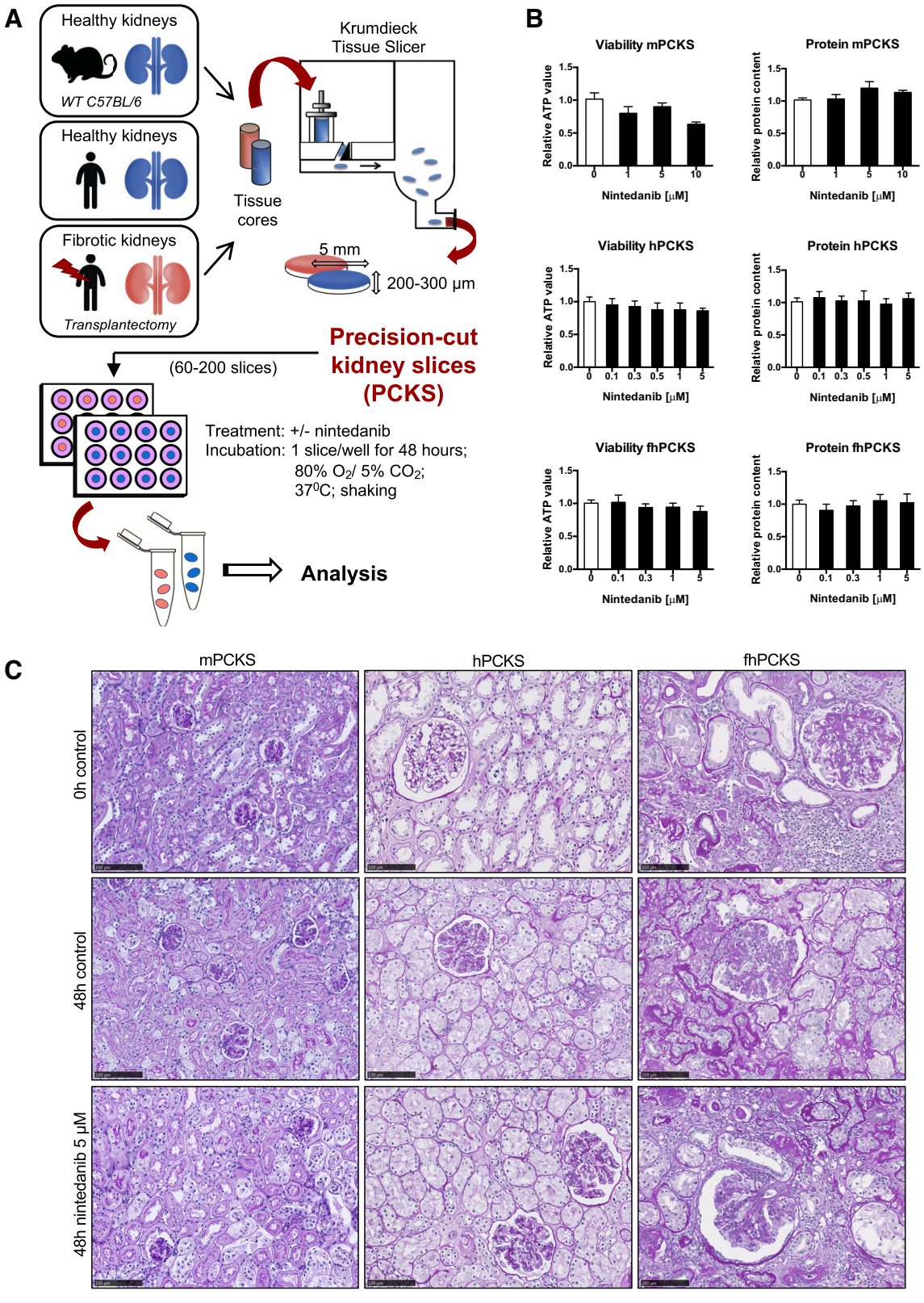

Western Blot Analysis

Total protein was extracted from PCKS with ice-cold RIPA buffer (Thermo Scientific, Waltham, MA) supplemented with a protease inhibitor cocktail and PhosStop (Sigma-Aldrich, St. Louis, MO). A total of 80–100 μg of protein was separated via SDS-PAGE using 10% polyacrylamide gels and blotted onto polyvinylidene fluoride membranes (Trans-Blot Turbo Transfer System, Bio-Rad, Veenendal, The Netherlands). 2,2,2-Trichloroethanol (TCE; Sigma-Aldrich) allowed for visible detection of total protein load (22). Membranes were blocked in 5% nonfat milk and Tris-buffered saline-Tween 20 (Bio-Rad) and incubated with primary antibody (Supplemental Table S3) overnight at 4°C followed by incubation with the appropriate horseradish peroxidase-conjugated secondary antibody. Protein bands were visualized using Clarity Western ECL Substrate (Bio-Rad) and ChemiDoc Touch Imaging System (Bio-Rad). Protein expression was corrected for total protein and expressed as the relative value to the control group.

Phosphoproteomic Analysis of RTKs by Multiplex

A human RTK phosphoprotein magnetic bead panel (Merck Millipore, Billerica, MA) was used according to the manufacturer's instructions. Total protein was extracted using the supplied lysis buffer supplemented with protease inhibitor cocktail. Samples were diluted to a concentration of 1.5 μg/μL and passed through a 0.45 μm syringe filter (Whatman, Maidstone, UK). Detection was performed with the MAGPIX Multiplexing Instrument (Luminex, Austin, TX). Mean fluorescent intensity was used for quantification.

Histology

PCKS were fixed in 4% buffered formalin, embedded in paraffin, and sectioned 2 μm thickness. Tissue damage and renal fibrosis were assessed by periodic acid-Schiff (PAS) and picrosirius red (PSR) staining. Additionally, we performed immunohistochemistry for Ki-67, α-smooth muscle actin (α-SMA), and collagen type

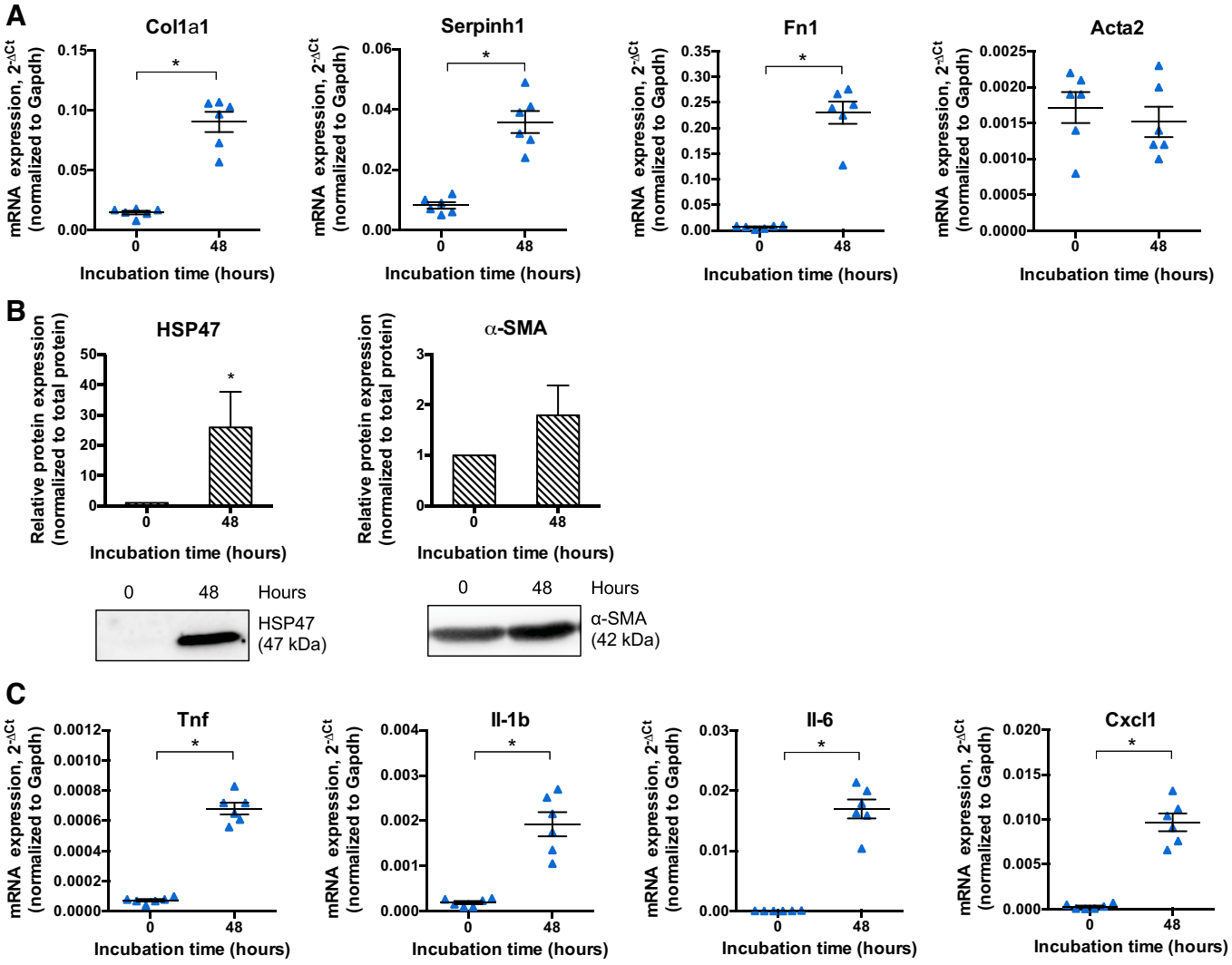

Fig. 2. Spontaneous fibrogenic and inflammatory response in murine precision-cut kidney slices (PCKS) during culture. *A*: mRNA expression of fibrosis markers. *B*: protein levels of heat shock protein 47 (HSP47) and α-smooth muscle actin (α-SMA) with representative Western blot images. *C*: mRNA expression of inflammation markers. Data are expressed as means ± SE; $n = 4–5$. Gene expression levels were compared using an unpaired Student's *t* test; protein levels were compared using a nonparametric Mann-Whitney test. *$P < 0.05$. Color code is as in Fig. 1. Acta2, α_2-smooth muscle actin; Col1a1, collagen type I-α_1; Cxcl1, chemokine (C-X-C motif) ligand 1; Fn1, fibronectin type 1; Serpinh1, serine proteinase inhibitor clade H (HSP47) member 1; Tnf, tumor necrosis factor.

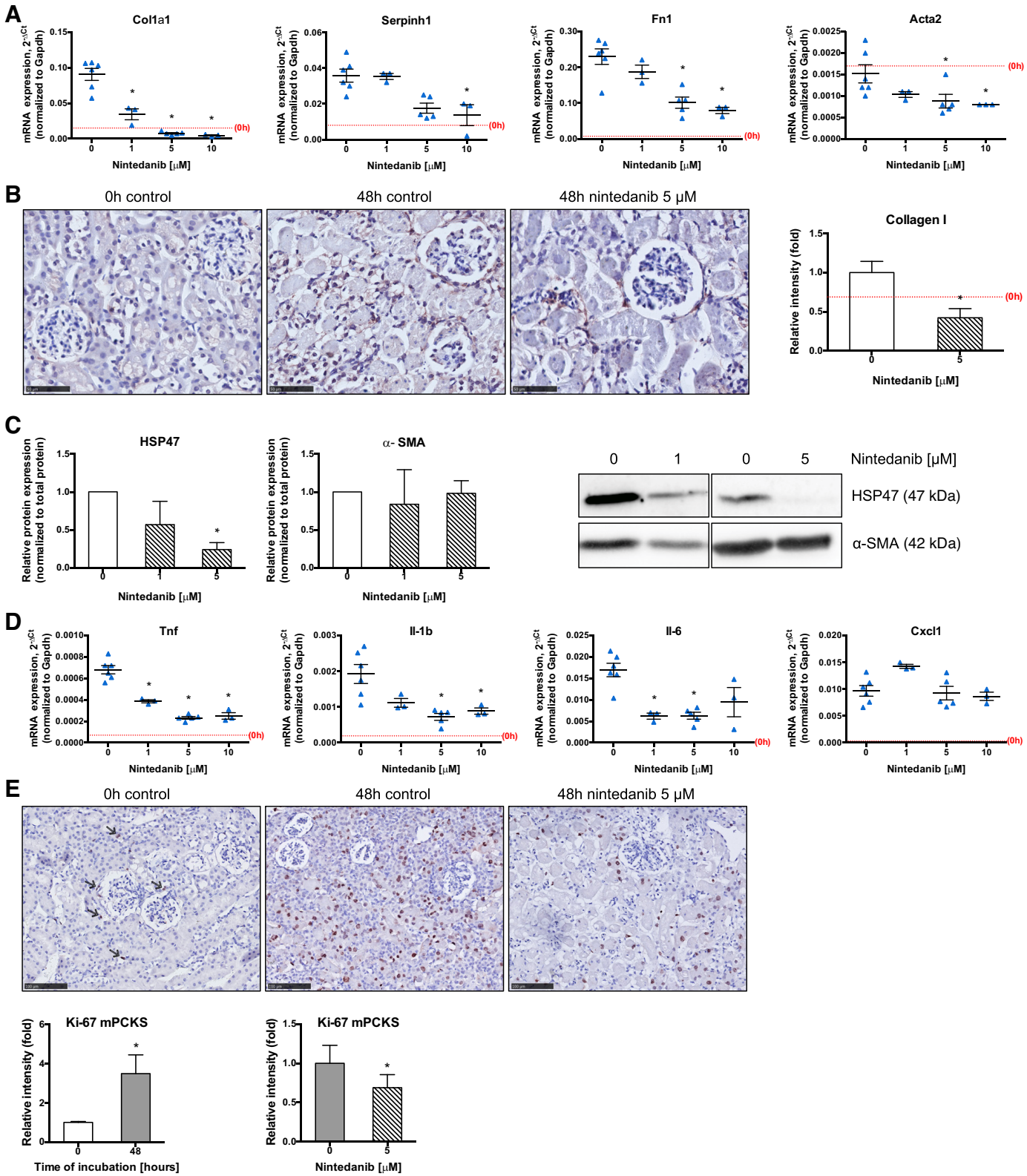

Fig. 3. Antifibrotic, anti-inflammatory, and antiproliferative effect of nintedanib in healthy mouse kidneys. Murine precision-cut kidney slices (mPCKS) were cultured in the presence of nintedanib (1, 5, or 10 μM) for 48 h. *A*: mRNA expression of fibrosis markers after 48-h incubation. *B*: representative sections with interstitial collagen type I accumulation visualized by immunohistochemistry (scale bar = 50 μm) and quantitative analysis of staining intensity. *C*: protein levels of heat shock protein 47 (HSP47) and α-smooth muscle actin (α-SMA) at 48 h with representative Western blot images. *D*: mRNA expression of inflammation markers after 48 h incubation. *E*: expression of cell proliferation marker Ki-67 in mPCKS during culture and after 48 h of treatment with 5 μM nintedanib was visualized by immunohistochemistry and quantified as relative intensity values. Data are expressed as means ± SE; $n = 3$–5. *$P < 0.05$. Color code is as in Fig. 1. Acta2, α_2-smooth muscle actin; Col1a1, collagen type I-α_1; Cxcl1, chemokine (C-X-C motif) ligand 1; Fn1, fibronectin type 1; Serpinh1, serine proteinase inhibitor clade H (HSP47) member 1; Tnf, tumor necrosis factor.

I. After deparaffinization and antigen retrieval with 0.1 M Tris-EDTA (pH 9.0) in a microwave oven for 15 min, tissue sections were blocked with 2% rat serum in PBS and 2% BSA for 10 min and then incubated with primary antibodies (Supplemental Table S3) for 1 h. The antibodies were localized using the appropriate horseradish peroxidase-conjugated secondary and tertiary antibodies and the ImmPact NovaRed kit (Vector, Burlingame, CA) followed by hematoxylin counterstaining. Stained tissue sections were scanned using a Nanozoomer Digital Pathology Scanner (NDP Scan U10074-01, Hamamatsu Photonics). To quantify the stained areas, whole slide images were processed with Aperio ImageScope (v12.3, Aperio Technologies, Vista, CA) by applying the Positive Pixel Count V9 algorithm (hue value set to 0). The intensities were measured as percentages (number of positive and strong positive pixels divided by the total number of pixels) and expressed as relative values to the control group.

Statistics

Results are expressed as means ± SE of a minimum of three independent experiments. Statistics were performed using GraphPad Prism 6.0 (GraphPad Software) by an unpaired Student's *t* test or one-way ANOVA followed by a Dunnett's multiple-comparisons test. The protein levels of heat shock protein (HSP)47 and α-SMA were compared using a nonparametric Kruskal-Wallis test followed by a Dunn's multiple-comparisons test. Differences be-

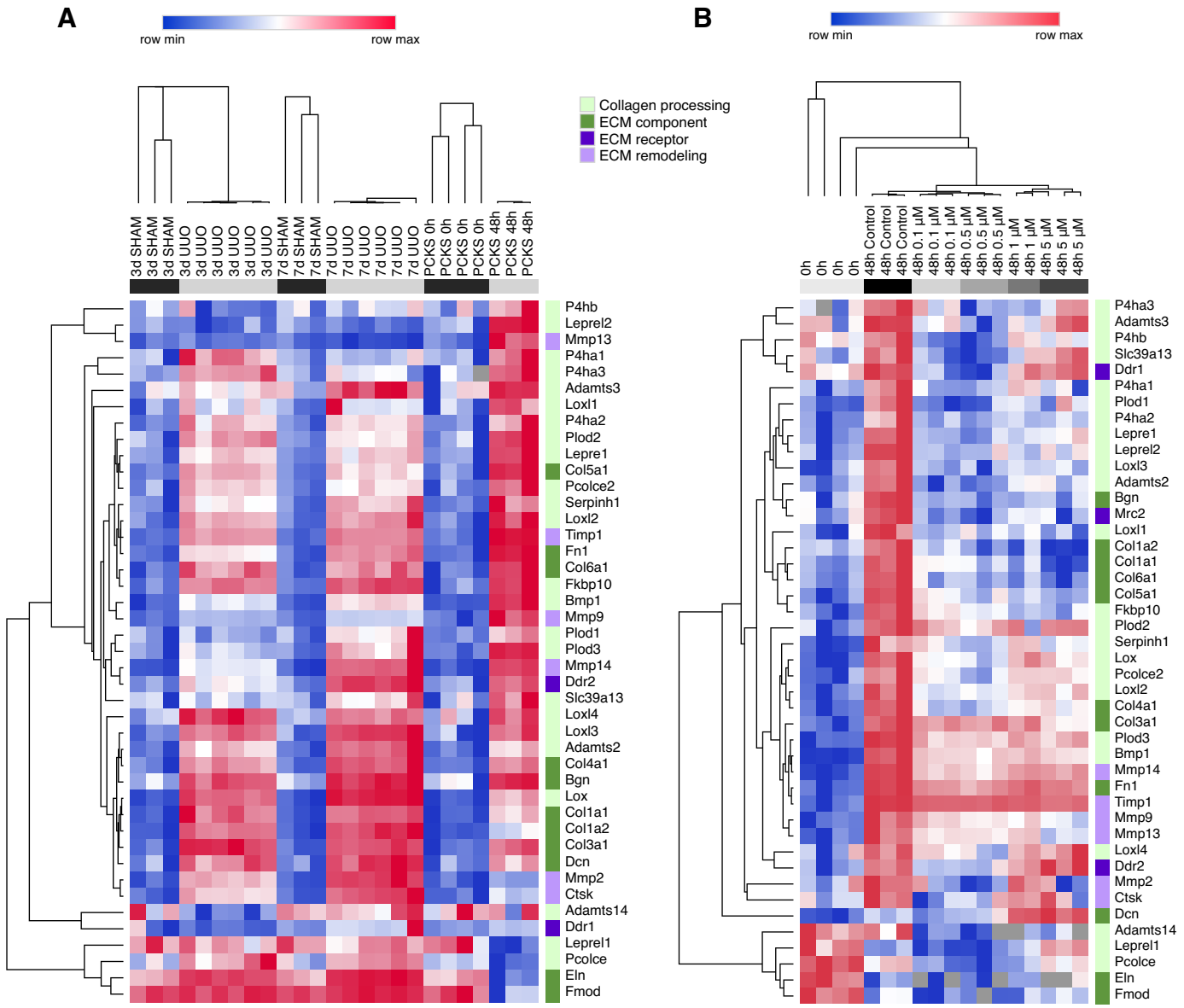

Fig. 4. Transcriptional changes in the extracellular matrix (ECM) homeostasis genes in murine precision-cut kidney slices (mPCKS) as measured by TaqMan low-density array. *A*: heatmap illustrating $\log_2$ fold changes in the expression of ECM-related genes in murine kidneys subjected to 3 days (3d) or 7 days (7d) of unilateral ureteral obstruction (UUO) and in mPCKS during 48-h culture. Fold changes are relative to the average expression in the corresponding control group (i.e., 3-day UUO relative to 3-day sham, 7-day UUO relative to 7-day sham, or 48-h mPCKS relative to 0-h mPCKS). *B*: heatmap of ECM modulation profiles in mPCKS at 0 h, 48 h, and treated with nintedanib (0.1–5 μM) for 48 h. Fold changes are relative to the average expression in the 0-h mPCKS group. Red and blue indicate relatively high and low expression, respectively (gray color indicates undetermined values). Average linkage hierarchical clustering (supervised in *A* and unsupervised in *B*) was performed using Pearson correlation. Complementary statistical analyses performed on Δthreshold cycle (C_t) values are shown in Supplemental Figs. S3 and S4. Full gene names are listed in Supplemental Table S2.

tween groups were considered to be statistically different when $P < 0.05$. For the low-density array heatmap, average linkage clustering was performed using Pearson correlation. The heatmap was generated using the online tool Morpheus (https://software.broadinstitute.org/morpheus/).

RESULTS

A brief summary of the study workflow is shown in Fig. 1*A*. Murine PCKS (mPCKS) and human PCKS (hPCKS) remained viable during 48 h of incubation, as reflected by unchanged ATP and total protein content (Fig. 1*B*). In addition, periodic acid-Schiff staining revealed typical structural changes in slices because of the culturing in accordance with previously reported results (34, 35). In particular, mPCKS and hPCKS from healthy kidneys showed signs of cellular damage (i.e., pyknosis and anucleosis), tubulointerstitial injury, and glomerular injury at 48 h. In turn, culture of human fibrotic PCKS (hfPCKS) induced further expansion of interstitial extracellular matrix (ECM), tubular atrophy, and glomerular sclerosis. Nintedanib at 5 μM showed no indication toward worsening of the morphology (Fig. 1*C*).

Nintedanib in mPCKS

Mitigation of fibrosis and inflammation by nintedanib. During 48-h incubation, spontaneous onset of fibrosis occurred in mPCKS, as reflected by an upregulation of mRNA levels of collagen type I, fibronectin, and HSP47 [encoded by *Col1a1*, fibronectin-1 (*Fn1*), and serine proteinase inhibitor clade H member 1 (*Serpinh1*), respectively] and by increased protein levels of HSP47 (Fig. 2, *A* and *B*). Nintedanib effectively mitigated fibrogenesis, as it clearly reduced *Col1a1* gene expression (Fig. 3*A*), with an IC_{50} value of 0.7 μM (Supplemental Fig. S1*A*). Furthermore, nintedanib reduced mRNA levels of Fn1 and α-SMA (*Acta2*) (IC_{50} values of 4.4 μM and 6.2 μM, respectively), whereas it affected Serpinh1 only at the highest concentration (IC_{50} value of 5.8 μM). Treatment with 5 μM nintedanib significantly decreased interstitial accumulation of collagen type I and protein expression of HSP47 but did not affect α-SMA (Fig. 3, *B* and *C*). Collagen mRNA and protein levels declined below baseline expression (at 0 h) when mPCKS were treated with 5 and 10 μM nintedanib. The spontaneous onset of fibrosis in mPCKS was accompanied by an inflammatory response after 48 h (Fig. 2*C*). We observed a significant decrease in mRNA levels of TNF, IL-1β, and IL-6 (encoded by *Tnf*, *Il-1β*, and *Il-6*, respectively) in the presence of nintedanib, whereas chemokine (C-X-C motif) ligand 1 (*Cxcl1*) expression was not affected (Fig. 3*D*).

Antiproliferative activity of nintedanib in mPCKS. Previous studies have reported the antiproliferative effects of nintedanib (15, 40, 41). We evaluated these effects in mPCKS by Ki-67 immunohistochemistry, a marker of cell proliferation (Fig. 3*E*). We observed a 3.5-fold culture-induced increase in proliferation that was ~30% attenuated by 5 μM nintedanib.

Low-density array for genes related to ECM homeostasis. To investigate whether the observed onset of fibrogenesis in mPCKS approximates in vivo fibrogenesis, we measured and compared the expression of 43 genes related to ECM homeostasis in kidneys from mice with renal injury induced by UUO and in mPCKS. Figure 4*A* shows that both obstruction of murine kidneys (for 3 or 7 days) and culture of mPCKS introduced considerable changes in the expression of ECM-related genes: the majority of the tested genes were upregulated in the obstructed kidneys and cultured mPCKS. We performed a detailed statistical analysis on a subset of these samples and compared transcriptional changes that occured during the obstruction of murine kidneys for 7 days and during 48 h culture of mPCKS (Fig. 5). The analysis revealed that 31 of 43 tested genes (72%) were regulated in the same direction (i.e., upregulated) in the UUO kidneys and mPCKS, whereas only three genes [elastin (*Eln*), fibromodulin (*Fmod*), and procollagen C-endopeptidase enhancer (*Pcolce*)] were regulated in the opposite direction. Additionally, seven genes were regulated during culture of mPCKS but not during 7-day UUO, including prolyl 4-hydroxylase-α_1 (*P4ha1*), prolyl 4-hydroxylase-α_3 (*P4ha3*), prolyl 4-hydroxylase-β (*P4hb*), leprecan-like 1 (*Leprel*), leprecan-like 2 (*Leprel2*), lysyl oxidase-like 1 (*Loxl1*), and matrix metalloproteinase (MMP)-13 (*Mmp13*)]. Among tested transcripts, only expression of ADAM metallopeptidase with thrombospondin type 1 motif 14 (*Adamts14*) was unaltered by the obstruction or culturing. Taken together, culturing of PCKS for 48 h induced changes in ECM homeostasis that, for the large part, mirrored changes observed in UUO kidneys, indicating that PCKS resemble in vivo fibrogenesis.

Next, we investigated the impact of nintedanib on mPCKS. Figure 4*B* shows that nintedanib manifested its inhibitory activity already at the lowest concentration (0.1 μM). A detailed statistical analysis of the subset of these samples showed that 0.1 μM nintedanib significantly reduced the expression of

Fig. 5. Detailed analysis of the transcriptional changes in the extracellular matrix (ECM) homeostasis determined by TaqMan low-density array in the unilateral ureteral obstruction (UUO) mouse kidneys and murine precision-cut kidney slices (mPCKS). *A*: heatmap that illustrates changes in the gene expression patterns (log_2 fold changes) in kidneys from mice subjected to 7-day (7d) UUO and in mPCKS cultured for 48 h, as these groups were included for the statistical analysis. Red and blue indicate relatively high and low expression, respectively (gray color indicates undetermined values). Supervised average linkage hierarchical clustering was performed using Pearson correlation. *B*: statistical analysis on the Δthreshold cycle (C_t) values of the transcriptional changes in ECM homeostasis in the murine kidneys obstructed for 7-day murine kidneys and in culture for 48-h mPCKS (as determined by TaqMan low-density array). Fold changes were calculated as relative to the corresponding control (i.e., 7-day UUO vs. 7-day sham or 48-h mPCKS vs. 0-h mPCKS). Fold changes in red indicate significant upregulation (with $P < 0.05$), fold changes in blue indicate significant downregulation (with $P < 0.05$), and fold changes in black indicate no significant regulation of a gene. Data are expressed as means ± SE; experimental groups (7-day UUO vs. 7-day sham or 48-h mPCKS vs. 0-h mPCKS) were compared by an unpaired two-tailed Student's *t* test. *C* and *D*: numbers of genes that were not regulated or statistically significantly altered in expression during 7-day UUO or during 48-h culture of mPCKS. Adamts, a disintegrin and metalloproteinase with thrombospondin motif; Plod, procollagen-lysine 2-oxoglutarate 5-dioxygenase 1; Bmp, bone morphogenetic protein; Timp, tissue inhibitor of metalloproteinase; Fkbp, FK506-binding protein; Bgn, biglycan; Dcn, decorin; Ctsk, cathepsin K; Ddr, discoidin domain receptor; Eln, elastin; Fmod, fibromodulin; Fn, fibronectin; Lepre, leprecan; Leprel, leprecan-like; Lox, lysyl oxidase; Loxl, lysyl oxidase-like; Mmp, matrix metalloproteinase; P4h, prolyl 4-hydroxylase; Pcolce, procollagen C-endopeptidase enhancer; Serpinh1, serine proteinase inhibitor clade H (heat shock protein 47) member 1; Slc, solute carrier; Tnf, tumor necrosis factor.

80% of the tested ECM-related genes, including collagen subtypes *Col1a1*, *Col1a2*, *Col3a1*, *Col4a1*, *Col5a1*, and *Col6a1* and ECM degradation MMPs encoded by *Mmp2*, *Mmp9*, and *Mmp13* (Fig. 6). In turn, treatment of mPCKS with nintedanib at 5 μM significantly inhibited only 59% of ECM-related transcripts. This was accompanied by the observation that at high concentrations (1 and 5 μM) nintedanib regulated different mRNA clusters than at lower concentrations (0.1 and

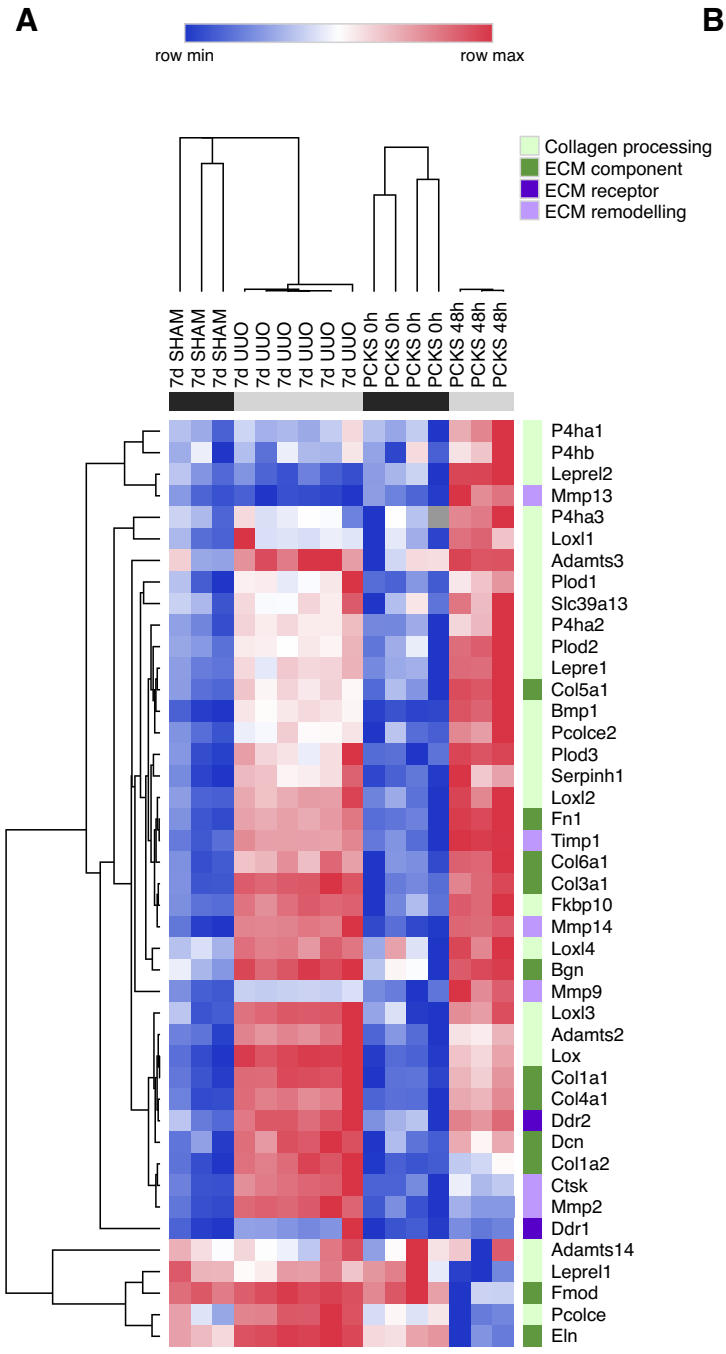

B

	UUO for 7 days *Fold change relative to 7d SHAM*	mPCKS in culture *Fold change relative to 0h PCKS*
Extracellular matrix component		
Col1a1	**21.47 ± 1.77**	**8.98 ± 1.39**
Col1a2	**16.35 ± 1.74**	**3.34 ± 0.51**
Col3a1	**16.27 ± 1.19**	**13.93 ± 2.26**
Col4a1	**5.95 ± 0.53**	**4.42 ± 0.34**
Col5a1	**3.49 ± 0.23**	**11.45 ± 0.99**
Col6a1	**4.48 ± 0.44**	**7.34 ± 0.82**
Fn1	**14.57 ± 1.41**	**41.32 ± 2.79**
Eln	**3.44 ± 0.17**	**0.11 ± 0.03**
Dcn	**3.71 ± 0.22**	**2.40 ± 0.24**
Bgn	**4.09 ± 0.19**	**4.07 ± 0.22**
Fmod	**1.38 ± 0.07**	**0.11 ± 0.04**
Collagen processing		
Plod1	**1.94 ± 0.31**	**2.10 ± 0.18**
Plod2	**1.90 ± 0.10**	**3.84 ± 0.34**
Plod3	**2.62 ± 0.44**	**4.37 ± 0.10**
P4ha1	1.23 ± 0.10	**2.50 ± 0.37**
P4ha2	**2.07 ± 0.07**	**2.83 ± 0.71**
P4ha3	1.69 ± 0.27	**7.03 ± 1.72**
P4hb	1.07 ± 0.04	**1.37 ± 0.12**
Lepre1	**2.31 ± 0.15**	**4.54 ± 0.49**
Leprel1	0.89 ± 0.06	**0.42 ± 0.04**
Leprel2	0.84 ± 0.04	**3.20 ± 0.08**
Lox	**26.72 ± 1.16**	**8.49 ± 1.16**
Loxl1	1.76 ± 0.40	**2.71 ± 0.32**
Loxl2	**5.90 ± 1.04**	**9.91 ± 1.80**
Loxl3	**4.26 ± 0.20**	**3.56 ± 0.45**
Loxl4	**2.65 ± 0.11**	**3.21 ± 0.42**
Serpinh1	**4.05 ± 0.67**	**5.84 ± 1.88**
Adamts2	**6.71 ± 0.80**	**3.59 ± 0.44**
Adamts3	**2.42 ± 0.22**	**2.69 ± 0.07**
Adamts14	1.04 ± 0.13	0.91 ± 0.30
Bmp1	**7.39 ± 0.34**	**33.55 ± 4.96**
Pcolce	**1.90 ± 0.10**	**0.57 ± 0.06**
Pcolce2	**2.68 ± 0.17**	**6.17 ± 1.47**
Fkbp10	**8.76 ± 0.50**	**10.95 ± 1.53**
Slc39a13	**1.38 ± 0.09**	**1.73 ± 0.17**
Extracellular matrix remodelling		
Mmp2	**17.25 ± 1.48**	**1.84 ± 0.14**
Mmp9	**5.14 ± 0.23**	**133.62 ± 61.25**
Mmp13	0.64 ± 0.05	**23.62 ± 7.97**
Mmp14	**18.30 ± 2.98**	**21.41 ± 1.16**
Timp1	**158.96 ± 18.37**	**1234.88 ± 75.85**
Ctsk	**9.53 ± 1.01**	**2.28 ± 0.28**
Extracellular matrix protein receptor		
Ddr1	2.54 ± 2.29	**1.54 ± 0.06**
Ddr2	**5.66 ± 0.38**	**4.45 ± 0.37**

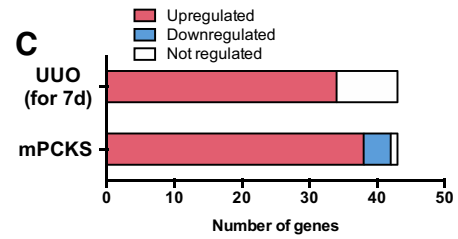

D

UUO for 7 days vs. mPCKS cultured for 48h	Number of genes	% of the total tested genes
Regulated in the same direction (*i.e.*, upregulated)	31	72
Regulated in the opposite direction	3	7
Not regulated in 7dUUO but regulated in mPCKS	7	16
Not regulated in 7dUUO and mPCKS	1	2

0.5 μM). In particular, seven genes (16%) were regulated significantly differently (i.e., not in the same direction) by nintedanib at 0.1 μM versus at 5 μM (Fig. 6*C*). Among these genes, *Adamts3*, *Pcolce*, *Slc39a13*, discoidin domain receptor 1 (*Ddr1*), and discoidin domain receptor 2 (*Ddr2*) were down-regulated by nintedanib at low concentrations but not regulated at high concentrations. Two transcripts, *Dcn* (encodes decorin) and *Leprel1*, "switched" their expression from unaltered or

A

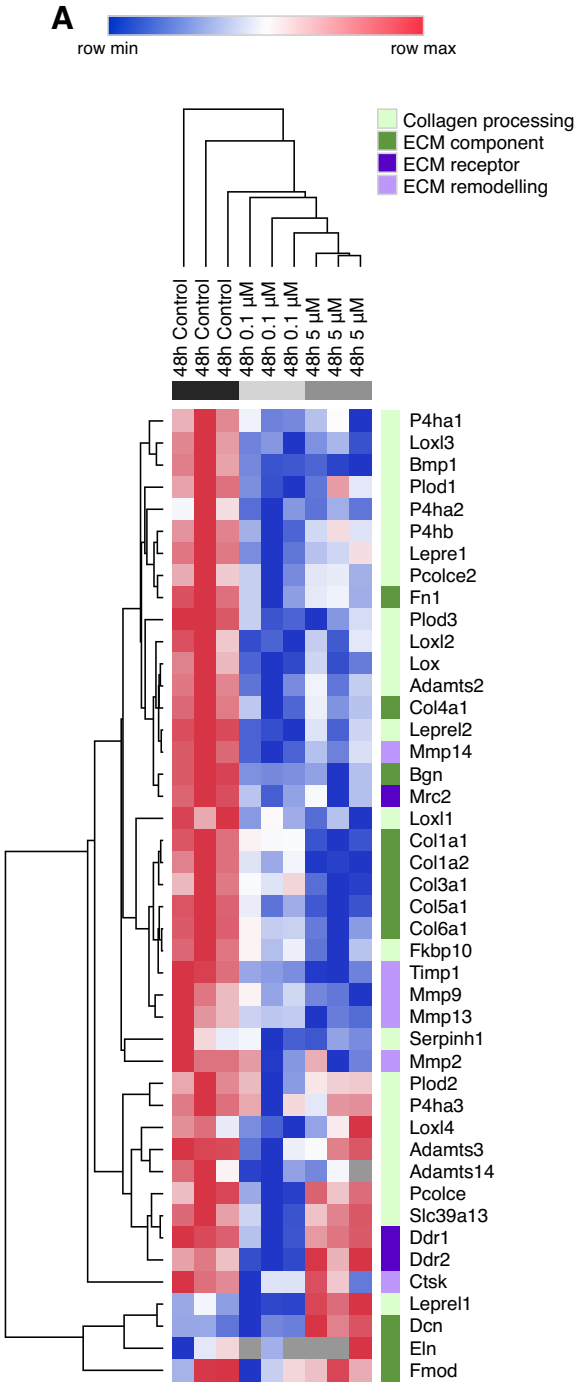

B

	Effect of nintedanib in mPCKS *Fold change relative to 48h control PCKS*		Regulation "switch"
	0.1 μM	5 μM	0.1 μM vs 5 μM
Extracellular matrix component			
Col1a1	0.24 ± 0.01	0.05 ± 0.00	*
Col1a2	0.32 ± 0.04	0.13 ± 0.00	*
Col3a1	0.59 ± 0.05	0.28 ± 0.02	*
Col4a1	0.36 ± 0.06	0.47 ± 0.04	ns
Col5a1	0.23 ± 0.05	0.13 ± 0.01	*
Col6a1	0.23 ± 0.03	0.10 ± 0.02	*
Fn1	0.34 ± 0.06	0.46 ± 0.03	ns
Eln	0.94 ± n.a.	2.98 ± n.a.	n.a.
Dcn	0.75 ± 0.12	**5.10 ± 0.73**	*
Bgn	0.24 ± 0.00	0.23 ± 0.05	ns
Fmod	0.38 ± 0.14	0.99 ± 0.23	ns
Collagen processing			
Plod1	0.45 ± 0.03	0.65 ± 0.12	ns
Plod2	0.60 ± 0.12	0.80 ± 0.02	ns
Plod3	0.57 ± 0.04	0.58 ± 0.05	ns
P4ha1	0.45 ± 0.06	0.45 ± 0.10	ns
P4ha2	0.46 ± 0.05	0.51 ± 0.04	ns
P4ha3	0.17 ± 0.13	0.41 ± 0.14	ns
P4hb	0.45 ± 0.05	0.65 ± 0.04	*
Lepre1	0.26 ± 0.03	0.46 ± 0.06	*
Leprel1	0.67 ± 0.01	**2.11 ± 0.11**	*
Leprel2	0.35 ± 0.01	0.48 ± 0.05	ns
Lox	0.35 ± 0.02	0.44 ± 0.06	ns
Loxl1	0.49 ± 0.05	0.38 ± 0.05	ns
Loxl2	0.26 ± 0.02	0.39 ± 0.07	ns
Loxl3	0.36 ± 0.04	0.39 ± 0.04	ns
Loxl4	0.52 ± 0.04	0.91 ± 0.23	ns
Serpinh1	0.43 ± 0.12	0.43 ± 0.04	ns
Adamts2	0.27 ± 0.03	0.39 ± 0.06	ns
Adamts3	0.33 ± 0.07	0.72 ± 0.12	*
Adamts14	0.18 ± 0.04	0.33 ± 0.09	ns
Bmp1	0.30 ± 0.02	0.26 ± 0.02	ns
Pcolce	0.48 ± 0.05	0.93 ± 0.07	*
Pcolce2	0.35 ± 0.07	0.50 ± 0.04	ns
Fkbp10	0.31 ± 0.04	0.15 ± 0.04	ns
Slc39a13	0.43 ± 0.07	0.91 ± 0.08	*
Extracellular matrix remodelling			
Mmp2	0.48 ± 0.15	0.45 ± 0.14	ns
Mmp9	0.17 ± 0.05	0.05 ± 0.01	ns
Mmp13	0.29 ± 0.01	0.13 ± 0.02	ns
Mmp14	0.33 ± 0.02	0.45 ± 0.04	*
Timp1	0.39 ± 0.01	0.30 ± 0.03	ns
Ctsk	0.35 ± 0.08	0.59 ± 0.24	ns
Extracellular matrix protein receptor			
Ddr1	0.38 ± 0.05	0.87 ± 0.05	*
Ddr2	0.31 ± 0.01	1.31 ± 0.21	*
Mrc2	0.24 ± 0.04	0.26 ± 0.07	ns

C

Effect of nintedanib in mPCKS	Number of genes	% of the total tested genes
Significantly inhibited by 0.1 μM nintedanib	35	80
Significantly inhibited by 5 μM nintedanib	26	59
Regulated differently (*i.e.*, not in the same direction) by 0.1 μM vs 5 μM nintedanib	7	16

downregulated after the treatment with 0.1 μM nintedanib to being upregulated by 5 μM nintedanib.

Nintedanib in Healthy Human PCKS

Targeted inhibition of gene expression and tyrosine kinase receptor activation. Culturing of the slices led to a significant downregulation of VEGF receptor (VEGFR)1, VEGFR2, and FGF receptor 2 (FGFR2) mRNA (Fig. 7*A*). Nintedanib already reduced expression of PDGFRβ, VEGFR1, and VEGFR3 in hPCKS at 0.1 μM (Fig. 7*B*). The treatment did not affect expression of VEGFR2; however, it increased FGFR2 expression at 5 μM.

Four phospho-RTKs (p-RTKs) were upregulated during incubation of hPCKS: p-PDGFRα, p-PDGFRβ, p-VEGFR1, and p-VEGFR2 (Fig. 7*C*). This suggests that the onset of fibrosis in healthy hPCKS was associated with the activation of PDGF and VEGF signaling pathways. Figure 7*D* shows that nintedanib reduced phosphorylation of p-PDGFRα and p-VEGFR1 at 0.3 μM (by 39.8% and 55%, respectively) and of PDGFRβ and VEGFR2 at 0.1 μM (by 45.3% and 23%). In contrast, the activation of VEGFR3 and FGFR1 in hPCKS was neither affected by 48-h incubation nor by treatment with nintedanib (Fig. 7, *C* and *D*).

Mitigation of fibrosis and inflammation markers by nintedanib. In line with previously published data (34), fibrogenesis was initiated during incubation of hPCKS, as revealed by the increase in *COL1A1* and *SERPINH1* transcription and protein levels of HSP47 (Fig. 8, *A* and *B*). Expression of *ACTA2* significantly dropped after 48 h, whereas *FN1* expression remained unchanged. Treatment with nintedanib resulted in a concentration-dependent inhibition of all tested fibrosis markers except for *ACTA2* (Fig. 9*A*). IC_{50} values were 0.6 μM for *COL1A1*, 1.5 μM for *SERPINH1*, and 1.7 μM for *FN1* (Supplemental Fig. S1*B*). Nintedanib at 5 μM reduced the accumulation of collagen type I to the baseline levels (at 0 h) and affected the protein level of HSP47 (Fig. 9, *B* and *C*). In concordance with gene expression, nintedanib had no influence on α-SMA expression.

Similar to mPCKS, a substantial increase in mRNA levels of cytokines, such as TNF, IL-1B, IL-6, and CXCL8/IL-8, occurred in hPCKS during the culture period (Fig. 8*C*). Nintedanib significantly reduced the expression of these inflammation markers at the highest tested concentration (5 μM; Fig. 9*D*). Interestingly, the IL-1B mRNA level was inhibited at 0.5 μM.

Antiproliferative activity of nintedanib in hPCKS. We observed comparable results of Ki-67 expression in hPCKS as in mPCKS: expression increased during culture (fold induction of 10.4) and nintedanib reduced proliferation by ~73% (Fig. 9*E*).

Nintedanib in Established Fibrosis PCKS

Characterization of fhPCKS. fhPCKS showed high basal gene expression of *COL1A1*, *SERPINH1*, and *FN1* as well as clear inflammatory profiles compared with healthy kidneys (Fig. 10, *A* and *B*). Histological analysis confirmed the fibrotic phenotype by showing an extensive tubular atrophy, ECM accumulation, and interstitial fibrosis (Fig. 10, *C* and *D*).

To analyze the processes occurring during culture of fhPCKS, we studied viability and gene expression up to 72 h. Similar to healthy hPCKS (34), the ATP content of fhPCKS increased during first 24 h, after which levels plateaued (Fig. 10*E*). As described above, healthy PCKS develop a fibrotic response during incubation. We observed a different pattern in fhPCKS: mRNA expression of COL1A1, SERPINH1, and FN1 remained unchanged (Fig. 10*F*). On the other hand, elevated collagen type I deposition and highly increased protein expression of HSP47 might indicate that fibrogenesis was still ongoing during incubation (Fig. 10, *G* and *H*). Similar to hPCKS, *ACTA2* expression dropped in fhPCKS during culture, whereas α-SMA protein expression remained unchanged. Regarding the inflammation markers, fhPCKS showed unaffected gene expression of *TNF* and *IL-1B* during culture. Levels of *IL-6* and *CXCL8/IL-8* increased at 24 h and then gradually declined (Fig. 10*I*).

Effect of nintedanib on fibrosis and inflammation markers. Treatment of fhPCKS with nintedanib did not affect fibrosis markers on gene expression. Only the highest tested concentration (5 μM) numerically, but not statistically significantly, reduced expression of *COL1A1* and *SERPINH1* (Fig. 11*A*). We detected nonsignificant effects on interstitial accumulation of collagen type I and protein expression of α-SMA; however, nintedanib at 5 μM significantly affected HSP47 (Fig. 11, *B* and *C*). Interestingly, 1 and 5 μM nintedanib downregulated

Fig. 6. Detailed analysis of the transcriptional changes in the expression of extracellular matrix-related genes in murine precision-cut kidney slices (mPCKS) treated with nintedanib for 48 h. *A*: heatmap illustrating changes in the gene expression patterns (log_2 fold changes) in mPCKS cultured in the absence of nintedanib or treated with nintedanib at 0.1 or 5 μM for 48 h, as these groups were included for the statistical analysis. Fold changes were calculated as relative to the average expression in the untreated mPCKS (48 h). Red and blue indicate relatively high and low expression, respectively (gray color indicates undetermined values). Unsupervised average linkage hierarchical clustering was performed using Pearson correlation. *B*: statistical analysis on the Δthreshold cycle (C_t) values of the transcriptional changes in the expression of extracellular matrix (ECM)-related genes in mPCKS after treatment with nintedanib at the lowest (0.1 μM) and highest (5 μM) tested concentration (as determined by TaqMan low-density array). Fold changes were calculated as relative to the untreated slices (48 h). Fold changes in blue indicate significant downregulation (with $P < 0.05$), fold changes in red indicate significant upregulation (with $P < 0.05$), and fold changes in black indicate no significant change in the expression of a gene. Data are expressed as means ± SE; experimental groups (48-h untreated mPCKS, mPCKS treated with 0.1 μM nintedanib, and mPCKS treated with 5 μM nintedanib) were compared by one-way ANOVA followed by a Dunnett's multiple-comparisons test. *Statistical differences between mPCKS treated with 0.1 vs. 5 μM nintedanib. The red asterisks indicate genes that were considered as "switched" in their expression between 0.1 and 5 μM nintedanib treatment groups. *C*: numbers of genes that were statistically significantly inhibited by nintedanib (0.1 and 5 μM) as well as numbers of genes that "switched" their expression when mPCKS were exposed to the highest tested concentration of nintedanib compared with the lowest tested concentration. Adamts, a disintegrin and metalloproteinase with thrombospondin motif; Plod, procollagen-Lysine 2-oxoglutarate 5-dioxygenase 1; Bmp, bone morphogenetic protein; Timp, tissue inhibitor of metalloproteinase; Fkbp, FK506-binding protein; Bgn, biglycan; Dcn, decorin; Ctsk, cathepsin K; Mrc, mannose receptor C type; Col, collagen; Ddr, discoidin domain receptor; Eln, elastin; Fmod, fibromodulin; Fn, fibronectin; Lepre, leprecan; Leprel, leprecan-like; Lox, lysyl oxidase; Loxl, lysyl oxidase-like; Mmp, matrix metalloproteinase; P4h, prolyl 4-hydroxylase; Pcolce, procollagen C-endopeptidase enhancer; Serpinh1, serine proteinase inhibitor clade H (heat shock protein 47) member 1; Slc, solute carrier; ns, not significant; n.a., not available (e.g., because of undetermined values).

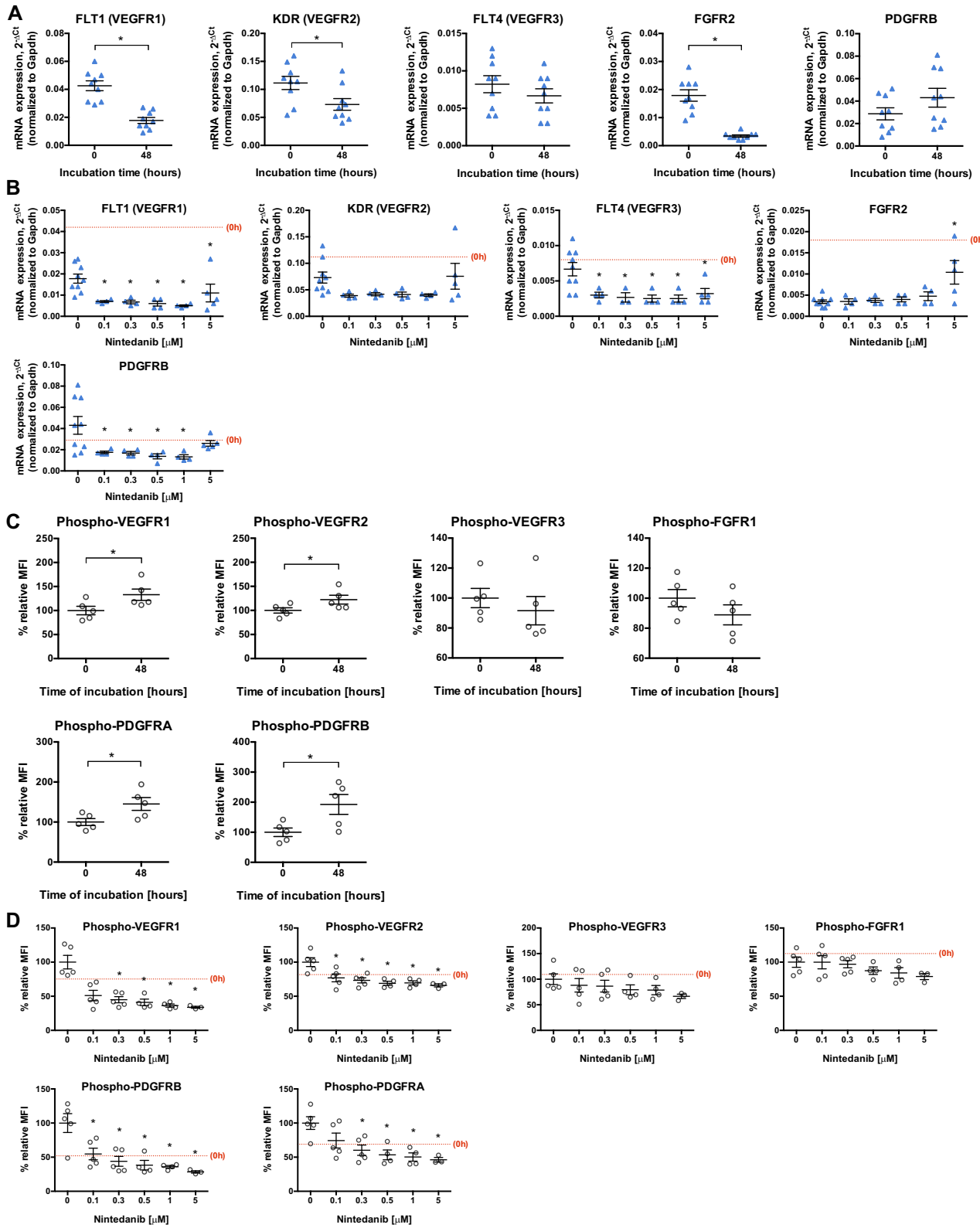

Fig. 7. Tyrosine kinase receptor (RTK) expression and activation in human precision-cut kidney slices (hPCKS) after 48-h culture and after nintedanib treatment. *A*: RTK mRNA expression in hPCKS after 48-h culture, as measured by real-time quantitative PCR. *B*: RTK mRNA expression in hPCKS after 48-h treatment with nintedanib (0.1–5 μM). Blue color in *A* and *B* indicates that kidney slices were prepared from healthy tissue. *C*: phosphorylation of RTKs in hPCKS was measured by multiplex magnetic bead assay and expressed as relative mean fluorescence intensity (MFI) to the 0-h control. *D*: phosphorylation of RTKs in hPCKS treated with nintedanib (0.1–5 μM) for 48 h, shown as mean MFI relative to untreated hPCKS. Data are expressed as means ± SE; $n = 4–5$. *$P < 0.05$. FGFR, fibroblast growth factor receptor; FLT, Fms-related tyrosine kinase; KDR, kinase insert domain receptor; PDGFRA, platelet-derived growth factor receptor α; PDGFRB, platelet-derived growth factor receptor β; VEGFR, vascular endothelial growth factor receptor.

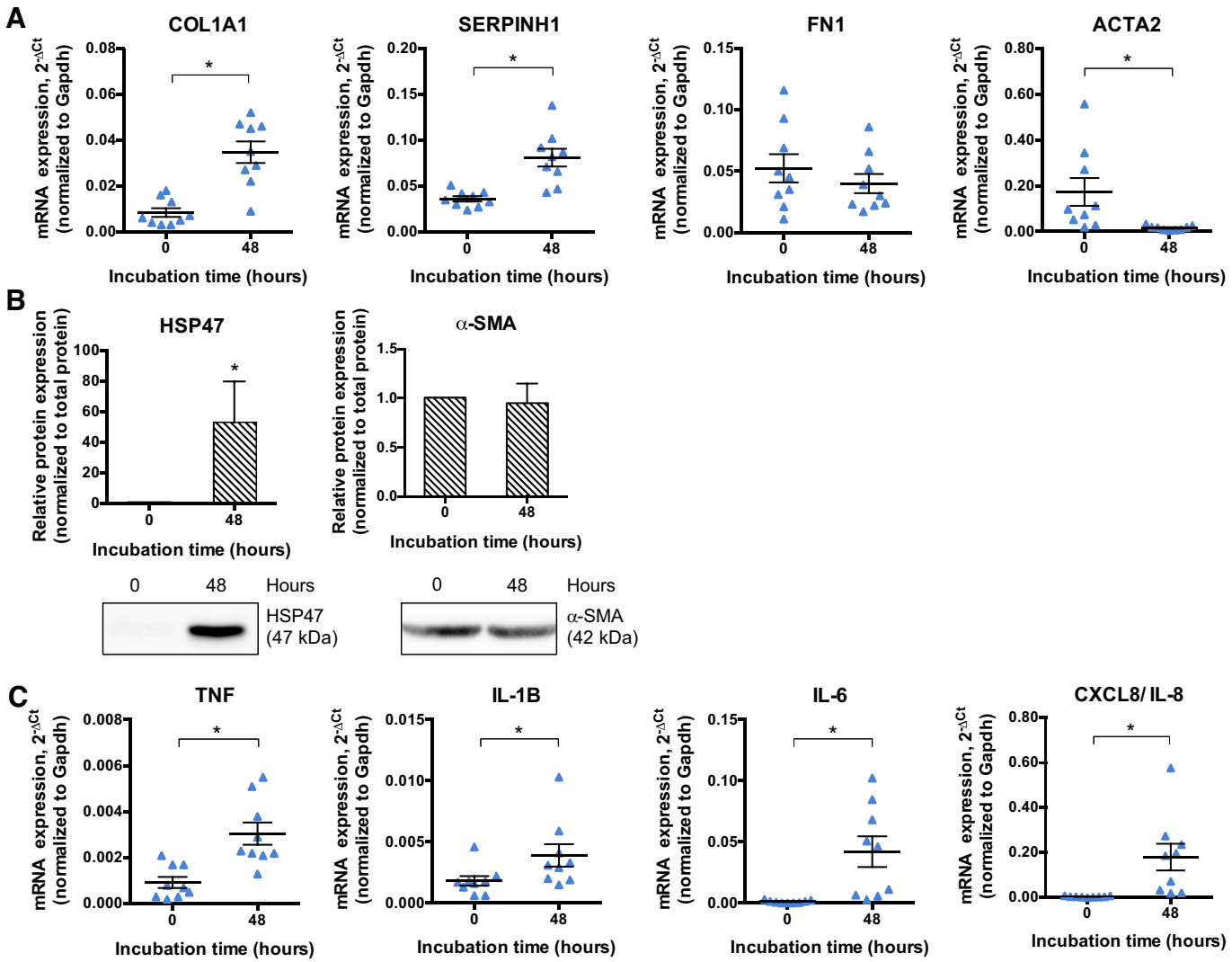

Fig. 8. Spontaneous fibrogenic and inflammatory response in human precision-cut kidney slices during culture. *A*: mRNA expression of fibrosis markers. *B*: protein levels of heat shock protein 47 (HSP47) and α-smooth muscle actin (α-SMA) with representative Western blot images. *C*: mRNA expression of inflammation markers. Data are expressed as means ± SE; $n = 4–5$. Gene expression levels were compared using an unpaired Student's *t* test; protein levels were compared using a nonparametric Mann-Whitney test. *$P < 0.05$. ACTA2, α_2-smooth muscle actin; COL1A1, collagen type I-α_1; CXCL8, chemokine (C-X-C motif) ligand 8; FN1, fibronectin type 1; SERPINH1, serine proteinase inhibitor clade H (heat shock protein 47) member 1; TNF, tumor necrosis factor.

IL-1B in fhPCKS by 82.5% and 86.3%, respectively (Fig. 11*D*).

Antiproliferative activity of nintedanib in fhPCKS. Similar to hPCKS, culture for 48 h induced Ki-67 expression in fhPCKS (Fig. 11*E*), whereas nintedanib inhibited cell proliferation by ~48%.

DISCUSSION

PCKS provide a unique opportunity to translate the obtained results from rodent models to human models, which is important for clinical drug development (38). In the present study, we expanded the experimental application of PCKS: we used healthy renal tissue of murine and human origin and explored PCKS from human fibrotic renal tissue as a model of established fibrosis. With this translational ex vivo model, we investigated the effects of nintedanib in healthy and diseased tissue. The PCKS model replicates some of the main characteristics of CKD, such as cellular damage, tubulointerstitial fibrosis, (local) inflammation, accumulation of ECM proteins, and dysregulated matrix turnover, as shown in this study and as previously reported by others (30, 34, 35). We demonstrated that spontaneous induction of fibrogenesis in PCKS resembles in vivo fibrogenesis, making this model suitable to study the mechanism of action and efficacy of antifibrotic compounds. We showed that nintedanib blocks the expression and phosphorylation of tyrosine kinase receptors and inhibits cell proliferation. Additionally, nintedanib attenuated the onset of fibrosis not only in mPCKS but also in hPCKS, although reversal of established fibrosis could not be achieved.

Nintedanib engaged its intended targets in human kidneys: it inhibited gene expression of PDGFRβ, VEGFR1, and VEGFR3 as well as culture-induced phosphorylation of PDGFRα, PDGFRβ, VEGFR1, and VEGFR2 starting at 0.1 μM, a concentration that is in the range of its maximum human exposure of 0.07 μM in patients with idiopathic pulmonary fibrosis after standard dosing (3a, 11, 28). The attenuation of PDGFRα and PDGFRβ

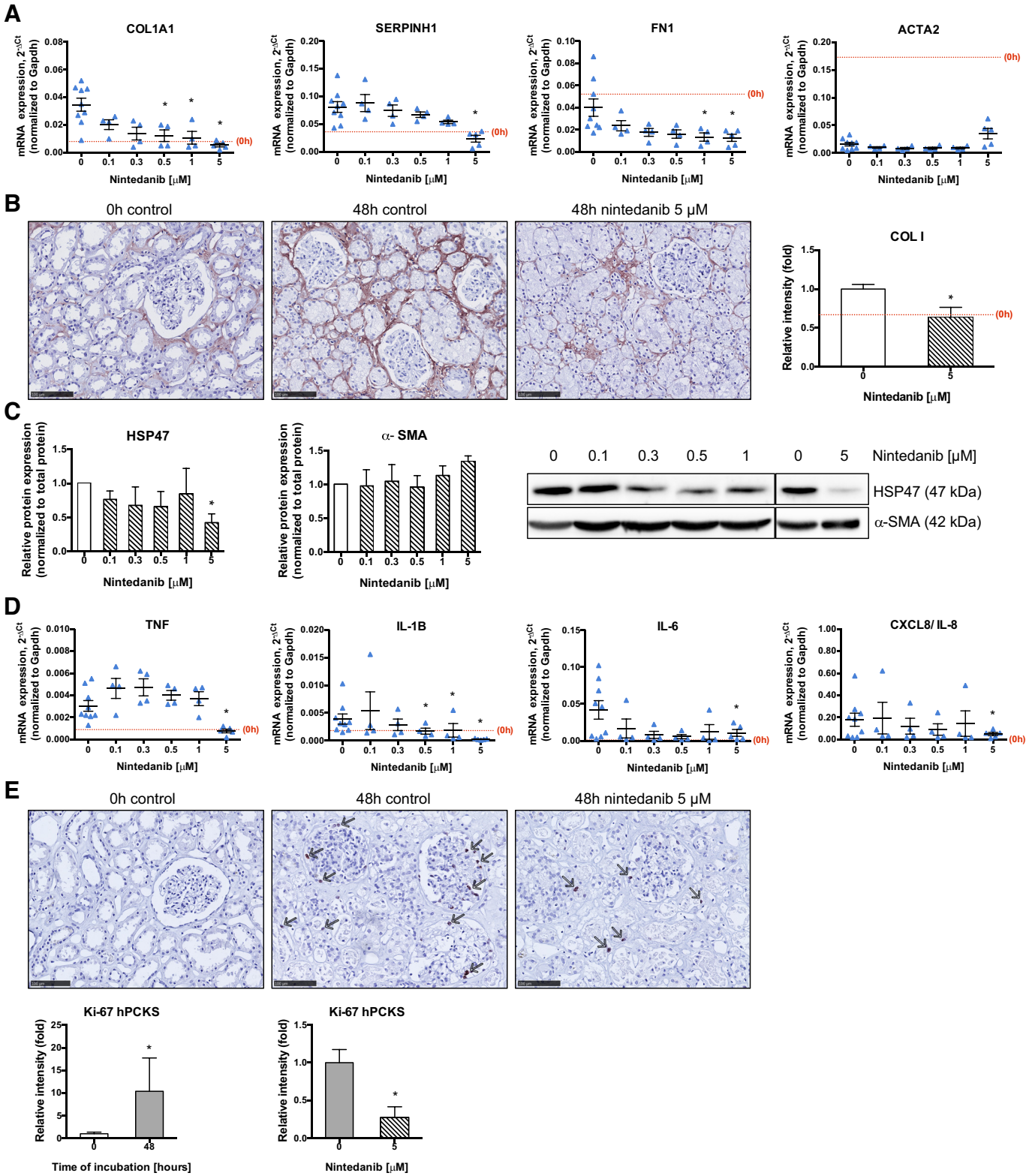

Fig. 9. Effects of nintedanib in healthy human kidneys. Human precision-cut kidney slices (hPCKS) were cultured in the presence of nintedanib (0.1–5 μM) for 48 h. *A*: mRNA expression of fibrosis markers after 48-h incubation. *B*: representative sections with interstitial collagen type I accumulation visualized by immunohistochemistry (scale bar = 100 μm) and quantitative analysis of staining intensity. *C*: protein levels heat shock protein 47 (HSP47) and α-smooth muscle actin (α-SMA) at 48 h with representative Western blot images. *D*: mRNA expression of inflammation markers after 48-h incubation. *E*: expression of cell proliferation marker Ki-67 in hPCKS during culture and after 48-h treatment with 5 μM nintedanib was visualized by immunohistochemistry and quantified as relative intensity values. Data are expressed as means ± SE; $n = 4–5$. *$P < 0.05$. ACTA2, α_2-smooth muscle actin; COL1A1, collagen type I-α_1; CXCL8, chemokine (C-X-C motif) ligand 8; FN1, fibronectin type 1; SERPINH1, serine proteinase inhibitor clade H (heat shock protein 47) member 1; TNF, tumor necrosis factor.

signaling by nintedanib is of therapeutic interest for renal fibrosis, as PDGF signaling leads to the differentiation of pericytes and resident fibroblasts to profibrotic ECM-producing myofibroblasts (9). The literature presents conflicting results on the role of VEGFR signaling in fibrosis and peritubular capillary restoration (2, 20, 24, 27). Therefore, beneficial inhibition of VEGFR signaling by nintedanib in renal fibrosis is subject to further studies.

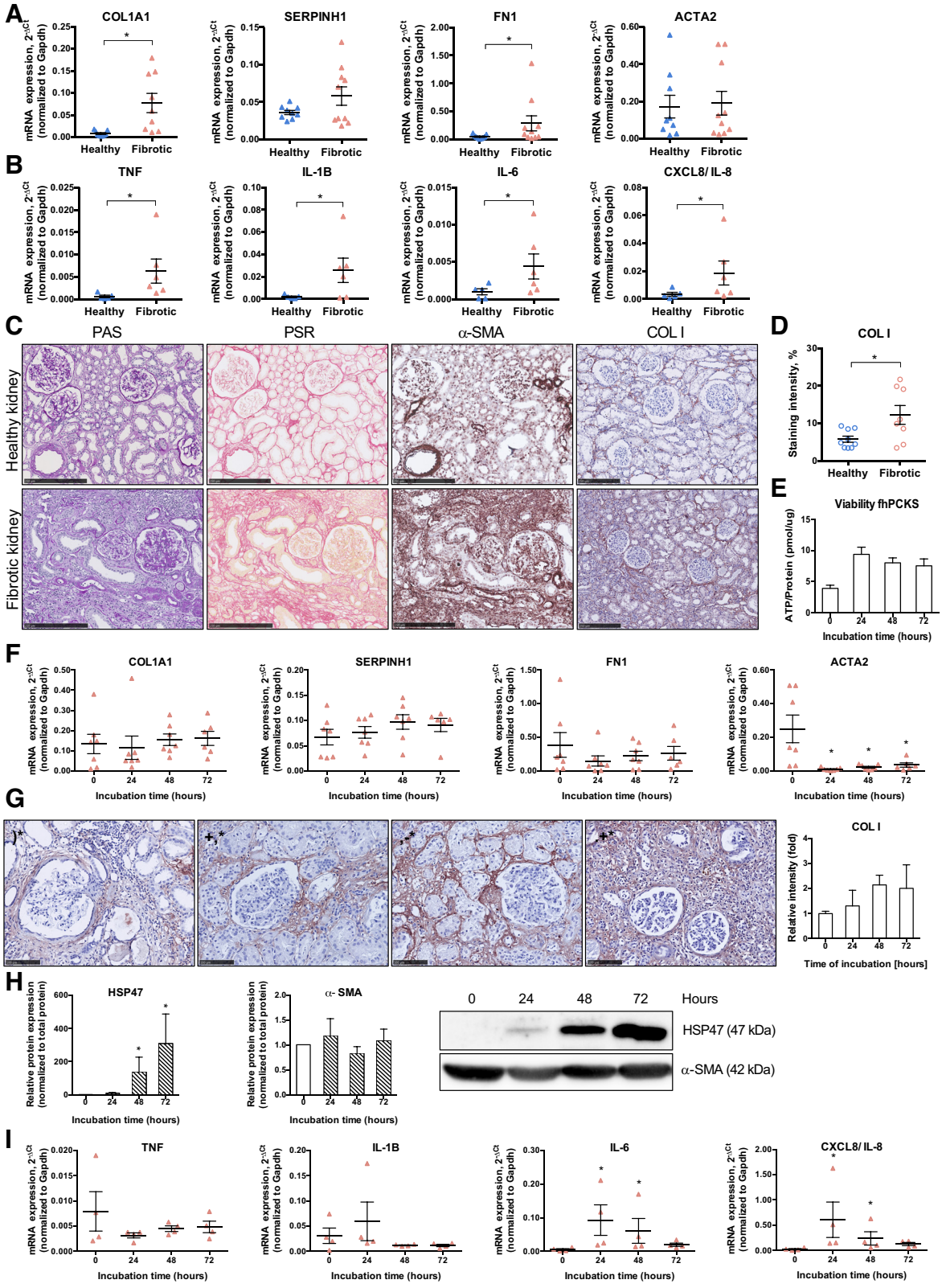

The inhibitory effects of nintedanib on RTKs were investigated by Liu et al. (25) in a UUO mouse model. They reported that nintedanib effectively blocked UUO-induced phosphorylation of PDGFRβ, VEGFR2, FGFR1, and FGFR2. In hPCKS, both FGFR1 and FGFR2 were not affected by nintedanib, possibly because of the differences in fibrogenic processes in murine and human tissues.

PCKS develop an early inflammatory response during culture followed by the onset of fibrosis (34). Nintedanib exerted anti-inflammatory activity in mPCKS and hPCKS. The observed effects are in line with earlier studies of nintedanib in mouse models of lung fibrosis (23, 40). This anti-inflammatory activity of nintedanib might translate into attenuation of renal injury.

Nintedanib also exerted antifibrotic effects in mPCKS and hPCKS, as demonstrated by a marked reduction of Col1a1 mRNA and protein expression. Furthermore, in mPCKS, nintedanib modulates ECM homeostasis even at the lowest concentration. Downregulation of these genes might lead to the altered secretion and fibril formation of collagen, as previously reported in primary human lung fibroblasts treated with transforming growth factor (TGF)-β (21). High concentrations of nintedanib regulate different mRNA clusters than low concentrations, reflected by a partial switch from inhibitory profile at 0.1 and 0.5 μM to the induction of some ECM-related genes at 1 and 5 μM. This could be explained by possible nonselective activity of nintedanib at high concentrations, whereas low concentrations have a more specific kinase-inhibitory profile (14). Despite the fact that nintedanib at 1 and 5 μM has an altered impact on ECM homeostasis, its overall effect remains antifibrotic.

The demonstrated attenuation of fibrosis concurs with previous results: nintedanib reduced lung fibrosis in bleomycin- or silica-treated mice and rats (1, 40, 41) and showed antifibrotic effects in various mouse models of systemic sclerosis (16, 17). Liu et al. (25) found that administration of nintedanib for 7 days after UUO injury attenuated renal fibrosis. Nintedanib inhibited TGF-β_1-induced renal fibroblast to myofibroblast transition and expression of ECM proteins in vitro in renal interstitial fibroblasts, indicating that nintedanib affects early events of TGF-β signaling. Wollin et al. (40, 41) also reported that nintedanib at higher concentrations possesses anti-TGF-β activity. We hypothesize that the observed antifibrotic effects of nintedanib in PCKS might be attributable to a combination of RTK inhibition and (perhaps nonselective) anti-TGF-β activity.

The cultures of mPCKS, hPCKS, and fhPCKS induced a strong spontaneous proliferative response, and, in line with published data (15, 40, 41), nintedanib effectively inhibited culture-induced cell proliferation in PCKS.

Our newly established translational PCKS model with tissue from fibrotic human kidneys showed a clear fibrotic phenotype compared with renal tissue from control donors. Culture of fhPCKS did not further increase the assessed markers of fibrosis, although an inflammatory peak was observed after the first day of culture. The preexisting fibrotic phenotype of fhPCKS might explain the difference with healthy PCKS.

Nintedanib showed diminished reduction in fibrosis markers in fhPCKS compared with hPCKS, most likely because of an increased interindividual variability (underlying primary renal disease, dialysis time, time since transplantation, and medication) in the fibrotic kidney slices. Nintedanib seems to be more effective in preventing or halting the onset of fibrosis in healthy PCKS rather than in reversing the established fibrosis, as modeled by fhPCKS. Our data in human diseased tissue is in conflict with the data in murine diseased tissue: delayed administration of nintedanib to UUO mice by Liu et al. (25) resulted in partial reversal of established renal fibrosis. However, even prolonged kidney obstruction in mice is not as severe as the late-stage fibrosis seen in patients with CKD, emphasizing the need for models that more closely resemble human pathology. PCKS, especially the culture of fhPCKS, can serve as a model for human CKD. Nevertheless, limitations of the ex vivo PCKS model are *1*) the relatively short culture period (48–72 h) is not always sufficient to detect posttranslational events, *2*) the availability of freshly resected human renal tissue is limited, *3*) interorgan interactions cannot be directly assessed, and *4*) circulating immune cells that contribute to the fibrogenesis are absent because slices lack blood circulation even though PCKS retain the native vascular network. Considering the significant role of infiltrating inflammatory cells and associated cytokines in renal fibrosis, a coculture system of PCKS with immune cells (or subsets of immune cells) can be established for future studies, which will better reflect the immunological interactions during the fibrogenic process in renal tissue.

Taken together, our results demonstrate the pharmacological effects of nintedanib in an ex vivo model of renal fibrosis, facilitating translation from animal studies to the clinic. Treatment of PCKS with nintedanib inhibited cell proliferation and attenuated the onset of inflammation and fibrosis, although reversal of established fibrosis could not be achieved. Nintedanib successfully inhibited PDGFR and VEGFR phosphorylation, demonstrating the potential use of these receptors as therapeutic targets to attenuate renal fibrosis. Therefore, along with the benefit of reducing animal use, hPCKS might provide direct and clinically relevant insights into human renal disease and therapeutic strategies.

Fig. 10. Characterization of fibrotic human precision-cut kidney slices (PCKS). PCKS were prepared from fibrotic human renal tissue obtained during end-stage renal disease nephrectomies or transplantectomies. *A*: baseline (prior incubation) mRNA expression of fibrosis markers in fibrotic compared with healthy tissue slices. *B*: baseline (prior incubation) mRNA expression of inflammation markers in fibrotic compared with healthy tissue slices. *C*: representative photomicrographs of human healthy and fibrotic PCKS before incubation (scale bar = 250 μm). Histological analyses by periodic acid-Schiff (PAS) and picrosirius red (PSR) staining showed extensive tubular atrophy and interstitial fibrosis, whereas α-smooth muscle actin (α-SMA) and collagen type I immunohistochemistry further confirmed the fibrotic phenotype. *D*: quantitative analysis of collagen type I immunohistochemistry in healthy and fibrotic PCKS (before incubation). *E*: viability of fibrotic PCKS during incubation presented as the average of picomoles of ATP per microgram of total protein. *F*: effect of incubation on mRNA expression of fibrosis markers. *G*: representative images of immunohistochemistry of collagen type I (scale bar = 100 μm) in fibrotic PCKS during 72-h culture with quantitative analysis. *H*: protein levels of heat shock protein (HSP47) and α-SMA ($n = 5$) during incubation with representative Western blot images. *I*: effect of incubation on mRNA expression of inflammation markers in fibrotic human PCKS (fhPCKS). Data are expressed as means ± SE; $n = 9$ for healthy PCKSs and $n = 8$–9 for fibrotic PCKSs. *$P < 0.05$. ACTA2, α_2-smooth muscle actin; COL1A1, collagen type I-α_1; CXCL8, chemokine (C-X-C motif) ligand 8; FN1, fibronectin type 1; SERPINH1, serine proteinase inhibitor clade H (heat shock protein 47) member 1; TNF, tumor necrosis factor.

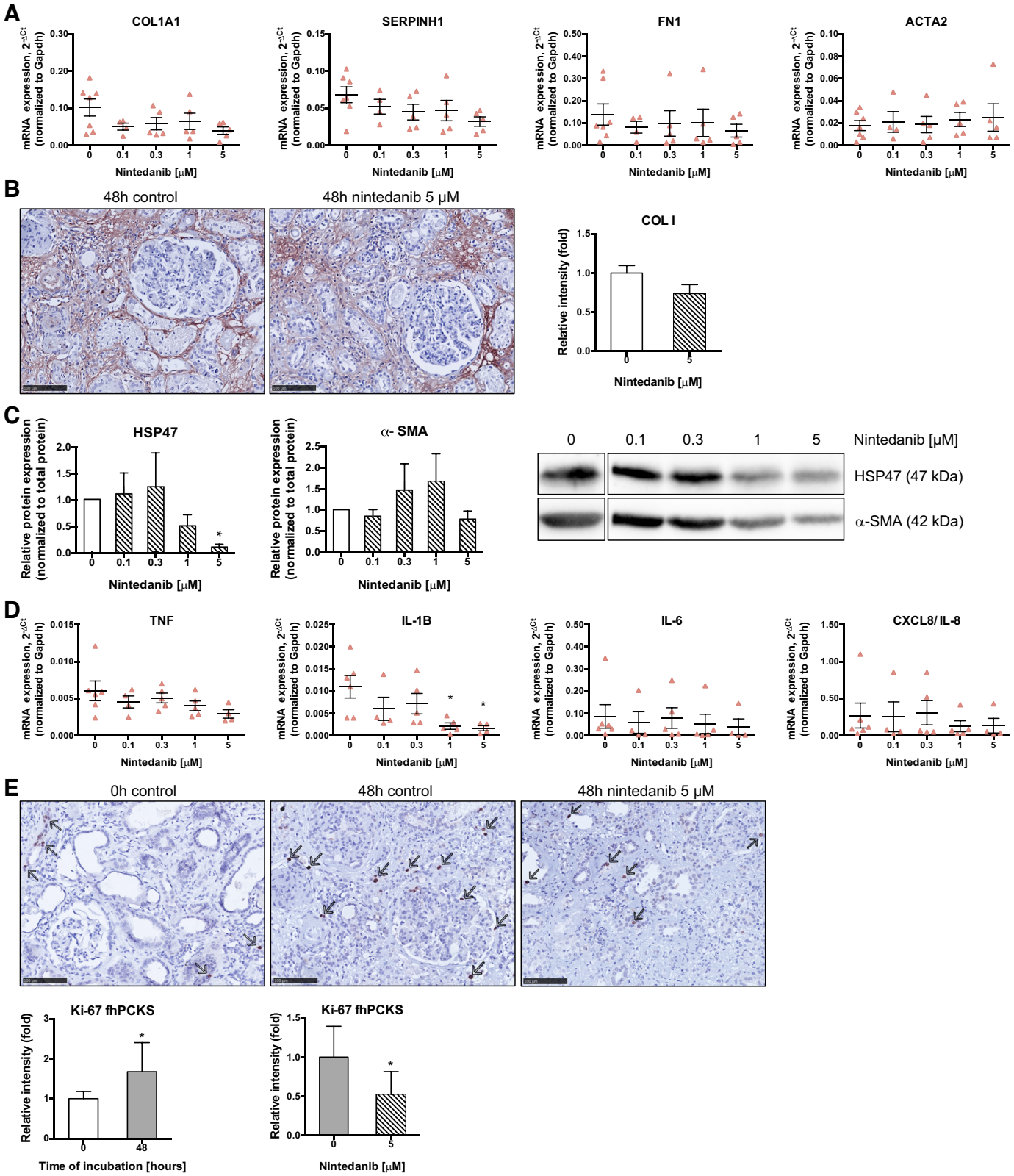

Fig. 11. Antifibrotic and anti-inflammatory effect of nintedanib in fibrotic human precision-cut kidney slices (fhPCKS). fhPCKS were cultured in the presence of nintedanib (0.1–5 μM) for 48 h. *A*: mRNA expression of fibrosis markers after 48-h incubation. *B*: representative sections with interstitial collagen type I accumulation visualized by immunohistochemistry (scale bar = 100 μm) and quantitative analysis of staining intensity. *C*: protein levels of heat shock protein 47 (HSP47) and α-smooth muscle actin (α-SMA) at 48 h with representative Western blot images. *D*: mRNA expression levels of inflammation markers after 48 h incubation. *E*: expression of cell proliferation marker Ki-67 in fhPCKS during culture and after 48-h treatment with 5 μM nintedanib was visualized by immunohistochemistry and quantified as relative intensity values. Data are expressed as means ± SE; $n = 4–5$. *$P < 0.05$. ACTA2, α_2-smooth muscle actin; COL1A1, collagen type I-α_1; CXCL8, chemokine (C-X-C motif) ligand 8; FN1, fibronectin type 1; SERPINH1, serine proteinase inhibitor clade H (HSP47) member 1; TNF, tumor necrosis factor.

ACKNOWLEDGMENTS

The authors thank the abdominal transplantation surgeons of the University Medical Center Groningen for providing the human renal tissue.

GRANTS

This work was kindly supported by ZonMw (the Netherlands Organization for Health Research and Development) Grant 114025003 and by Lundbeckfonden Grant R231-2016-2344 (to H. A. M. Mutsaers).

DISCLOSURES

L. Wollin is an employee of Boehringer Ingelheim Pharma. None of the other authors has any conflicts of interest, financial or otherwise, to disclose.

AUTHOR CONTRIBUTIONS

E.B., E.G.S., P.O., and M.B. conceived and designed research; E.B., E.G.S., B.P., A.M.L., I.J.d.J., R.A.B., H.v.G., L.W., and M.B. performed experiments; E.B., E.G.S., and M.B. analyzed data; E.B., E.G.S., and M.B. interpreted results of experiments; E.B. and E.G.S. prepared figures; E.B. and E.G.S. drafted manuscript; E.B., E.G.S., H.A.M., R.A.B., M.S., H.v.G., L.W., P.O., and M.B. edited and revised manuscript; E.B., E.G.S., H.A.M., B.P., A.M.L., I.J.d.J., R.A.B., M.S., H.v.G., L.W., P.O., and M.B. approved final version of manuscript.

REFERENCES

1. **Ackermann M, Kim YO, Wagner WL, Schuppan D, Valenzuela CD, Mentzer SJ, Kreuz S, Stiller D, Wollin L, Konerding MA.** Effects of nintedanib on the microvascular architecture in a lung fibrosis model. *Angiogenesis* 20: 359–372, 2017. doi:10.1007/s10456-017-9543-z.
2. **Bábíčková J, Klinkhammer BM, Buhl EM, Djudjaj S, Hoss M, Heymann F, Tacke F, Floege J, Becker JU, Boor P.** Regardless of etiology, progressive renal disease causes ultrastructural and functional alterations of peritubular capillaries. *Kidney Int* 91: 70–85, 2017. doi:10.1016/j.kint.2016.07.038.
3. **Beyer C, Distler JH.** Tyrosine kinase signaling in fibrotic disorders: translation of basic research to human disease. *Biochim Biophys Acta* 1832: 897–904, 2013. doi:10.1016/j.bbadis.2012.06.008.

3a. **Bonella F, Stowasser S, Wollin L.** Idiopathic pulmonary fibrosis: current treatment options and critical appraisal of nintedanib. *Drug Des Devel Ther* 9: 6407–6419, 2015. doi:10.2147/DDDT.S76648.

4. **Boor P, Ostendorf T, Floege J.** PDGF and the progression of renal disease. *Nephrol Dial Transplant* 29, *Suppl* 1: i45–i54, 2014. doi:10.1093/ndt/gft273.
5. **Buhl EM, Djudjaj S, Babickova J, Klinkhammer BM, Folestad E, Borkham-Kamphorst E, Weiskirchen R, Hudkins K, Alpers CE, Eriksson U, Floege J, Boor P.** The role of PDGF-D in healthy and fibrotic kidneys. *Kidney Int* 89: 848–861, 2016. doi:10.1016/j.kint.2015.12.037.
6. **Cernaro V, Trifirò G, Lorenzano G, Lucisano S, Buemi M, Santoro D.** New therapeutic strategies under development to halt the progression of renal failure. *Expert Opin Investig Drugs* 23: 693–709, 2014. doi:10.1517/13543784.2014.899352.
7. **Chen YT, Chang FC, Wu CF, Chou YH, Hsu HL, Chiang WC, Shen J, Chen YM, Wu KD, Tsai TJ, Duffield JS, Lin SL.** Platelet-derived growth factor receptor signaling activates pericyte-myofibroblast transition in obstructive and post-ischemic kidney fibrosis. *Kidney Int* 80: 1170–1181, 2011. doi:10.1038/ki.2011.208.
9. **Duffield JS.** Cellular and molecular mechanisms in kidney fibrosis. *J Clin Invest* 124: 2299–2306, 2014. doi:10.1172/JCI72267.
10. **Eisen T, Loembé AB, Shparyk Y, MacLeod N, Jones RJ, Mazurkiewicz M, Temple G, Dressler H, Bondarenko I.** A randomised, phase II study of nintedanib or sunitinib in previously untreated patients with advanced renal cell cancer: 3-year results. *Br J Cancer* 113: 1140–1147, 2015. doi:10.1038/bjc.2015.313.
11. **Eisen T, Shparyk Y, Macleod N, Jones R, Wallenstein G, Temple G, Khder Y, Dallinger C, Studeny M, Loembe AB, Bondarenko I.** Effect of small angiokinase inhibitor nintedanib (BIBF 1120) on QT interval in patients with previously untreated, advanced renal cell cancer in an open-label, phase II study. *Invest New Drugs* 31: 1283–1293, 2013. doi:10.1007/s10637-013-9962-7.
12. **Floege J, Eitner F, Alpers CE.** A new look at platelet-derived growth factor in renal disease. *J Am Soc Nephrol* 19: 12–23, 2008. doi:10.1681/ASN.2007050532.
13. **Genovese F, Kàrpàti ZS, Nielsen SH, Karsdal MA.** Precision-cut kidney slices as a tool to understand the dynamics of extracellular matrix remodeling in renal fibrosis. *Biomark Insights* 11: 77–84, 2016. doi:10.4137/BMI.S38439.
14. **Hilberg F, Roth GJ, Krssak M, Kautschitsch S, Sommergruber W, Tontsch-Grunt U, Garin-Chesa P, Bader G, Zoephel A, Quant J, Heckel A, Rettig WJ.** BIBF 1120: triple angiokinase inhibitor with sustained receptor blockade and good antitumor efficacy. *Cancer Res* 68: 4774–4782, 2008. doi:10.1158/0008-5472.CAN-07-6307.
15. **Hostettler KE, Zhong J, Papakonstantinou E, Karakiulakis G, Tamm M, Seidel P, Sun Q, Mandal J, Lardinois D, Lambers C, Roth M.** Anti-fibrotic effects of nintedanib in lung fibroblasts derived from patients with idiopathic pulmonary fibrosis. *Respir Res* 15: 157, 2014. doi:10.1186/s12931-014-0157-3.
16. **Huang J, Beyer C, Palumbo-Zerr K, Zhang Y, Ramming A, Distler A, Gelse K, Distler O, Schett G, Wollin L, Distler JH.** Nintedanib inhibits fibroblast activation and ameliorates fibrosis in preclinical models of systemic sclerosis. *Ann Rheum Dis* 75: 883–890, 2016. doi:10.1136/annrheumdis-2014-207109.
17. **Huang J, Maier C, Zhang Y, Soare A, Dees C, Beyer C, Harre U, Chen CW, Distler O, Schett G, Wollin L, Distler JH.** Nintedanib inhibits macrophage activation and ameliorates vascular and fibrotic manifestations in the Fra2 mouse model of systemic sclerosis. *Ann Rheum Dis* 76: 1941–1948, 2017. doi:10.1136/annrheumdis-2016-210823.
18. **Humphreys BD, Lin SL, Kobayashi A, Hudson TE, Nowlin BT, Bonventre JV, Valerius MT, McMahon AP, Duffield JS.** Fate tracing reveals the pericyte and not epithelial origin of myofibroblasts in kidney fibrosis. *Am J Pathol* 176: 85–97, 2010. doi:10.2353/ajpath.2010.090517.
19. **James MT, Hemmelgarn BR, Tonelli M.** Early recognition and prevention of chronic kidney disease. *Lancet* 375: 1296–1309, 2010. doi:10.1016/S0140-6736(09)62004-3.
20. **Kang DH, Joly AH, Oh SW, Hugo C, Kerjaschki D, Gordon KL, Mazzali M, Jefferson JA, Hughes J, Madsen KM, Schreiner GF, Johnson RJ.** Impaired angiogenesis in the remnant kidney model: I. Potential role of vascular endothelial growth factor and thrombospondin-1. *J Am Soc Nephrol* 12: 1434–1447, 2001.
21. **Knüppel L, Ishikawa Y, Aichler M, Heinzelmann K, Hatz R, Behr J, Walch A, Bächinger HP, Eickelberg O, Staab-Weijnitz CA; Inhibition of Collagen Fibril Assembly.** A novel antifibrotic mechanism of nintedanib and pirfenidone. *Am J Respir Cell Mol Biol* 57: 77–90, 2017. doi:10.1165/rcmb.2016-0217OC.
22. **Ladner CL, Yang J, Turner RJ, Edwards RA.** Visible fluorescent detection of proteins in polyacrylamide gels without staining. *Anal Biochem* 326: 13–20, 2004. doi:10.1016/j.ab.2003.10.047.
23. **Lee HY, Hur J, Kim IK, Kang JY, Yoon HK, Lee SY, Kwon SS, Kim YK, Rhee CK.** Effect of nintedanib on airway inflammation and remodeling in a murine chronic asthma model. *Exp Lung Res* 43: 187–196, 2017. doi:10.1080/01902148.2017.1339141.
24. **Lin SL, Chang FC, Schrimpf C, Chen YT, Wu CF, Wu VC, Chiang WC, Kuhnert F, Kuo CJ, Chen YM, Wu KD, Tsai TJ, Duffield JS.** Targeting endothelium-pericyte cross talk by inhibiting VEGF receptor signaling attenuates kidney microvascular rarefaction and fibrosis. *Am J Pathol* 178: 911–923, 2011. doi:10.1016/j.ajpath.2010.10.012.
25. **Liu F, Wang L, Qi H, Wang J, Wang Y, Jiang W, Xu L, Liu N, Zhuang S.** Nintedanib, a triple tyrosine kinase inhibitor, attenuates renal fibrosis in chronic kidney disease. *Clin Sci (Lond)* 131: 2125–2143, 2017. doi:10.1042/CS20170134.
26. **Livak KJ, Schmittgen TD.** Analysis of relative gene expression data using real-time quantitative PCR and the $2(-\Delta\Delta$ C(T)) Method. *Methods* 25: 402–408, 2001. doi:10.1006/meth.2001.1262.
27. **Long DA, Norman JT, Fine LG.** Restoring the renal microvasculature to treat chronic kidney disease. *Nat Rev Nephrol* 8: 244–250, 2012. doi:10.1038/nrneph.2011.219.
28. **Mross K, Stefanic M, Gmehling D, Frost A, Baas F, Unger C, Strecker R, Henning J, Gaschler-Markefski B, Stopfer P, de Rossi L, Kaiser R.** Phase I study of the angiogenesis inhibitor BIBF 1120 in patients with advanced solid tumors. *Clin Cancer Res* 16: 311–319, 2010. doi:10.1158/1078-0432.CCR-09-0694.
29. **Ostendorf T, Eitner F, Floege J.** The PDGF family in renal fibrosis. *Pediatr Nephrol* 27: 1041–1050, 2012. doi:10.1007/s00467-011-1892-z.
30. **Poosti F, Pham BT, Oosterhuis D, Poelstra K, van Goor H, Olinga P, Hillebrands J-L.** Precision-cut kidney slices (PCKS) to study development of renal fibrosis and efficacy of drug targeting ex vivo. *Dis Model Mech* 8: 1227–1236, 2015. doi:10.1242/dmm.020172.

31. **Remst DF, Blom AB, Vitters EL, Bank RA, van den Berg WB, Blaney Davidson EN, van der Kraan PM.** Gene expression analysis of murine and human osteoarthritis synovium reveals elevation of transforming growth factor β-responsive genes in osteoarthritis-related fibrosis. *Arthritis Rheumatol* 66: 647–656, 2014. doi:10.1002/art.38266.
32. **Roth GJ, Binder R, Colbatzky F, Dallinger C, Schlenker-Herceg R, Hilberg F, Wollin S-L, Kaiser R.** Nintedanib: from discovery to the clinic. *J Med Chem* 58: 1053–1063, 2015. doi:10.1021/jm501562a.
33. **Stribos EG, Hillebrands J-L, Olinga P, Mutsaers HA.** Renal fibrosis in precision-cut kidney slices. *Eur J Pharmacol* 790: 57–61, 2016. doi:10.1016/j.ejphar.2016.06.057.
34. **Stribos EG, Luangmonkong T, Leliveld AM, de Jong IJ, van Son WJ, Hillebrands JL, Seelen MA, van Goor H, Olinga P, Mutsaers HA.** Precision-cut human kidney slices as a model to elucidate the process of renal fibrosis. *Transl Res* 170: 8–16.e1, 2016. doi:10.1016/j.trsl.2015.11.007.
35. **Stribos EG, Seelen MA, van Goor H, Olinga P, Mutsaers HA.** Murine precision-cut kidney slices as an *ex vivo* model to evaluate the role of transforming growth Factor-β1 signaling in the onset of renal fibrosis. *Front Physiol* 8: 1026, 2017. doi:10.3389/fphys.2017.01026.
36. **Strutz F, Zeisberg M, Hemmerlein B, Sattler B, Hummel K, Becker V, Müller GA.** Basic fibroblast growth factor expression is increased in human renal fibrogenesis and may mediate autocrine fibroblast proliferation. *Kidney Int* 57: 1521–1538, 2000. doi:10.1046/j.1523-1755.2000.00997.x.
37. **Tampe D, Zeisberg M.** Potential approaches to reverse or repair renal fibrosis. *Nat Rev Nephrol* 10: 226–237, 2014. doi:10.1038/nrneph.2014.14.
37a. **van Dijk F, Olinga P, Poelstra K, Beljaars L.** Targeted therapies in liver fibrosis: combining the best parts of platelet-derived growth factor BB and interferon gamma. *Front Med (Lausanne)* 2: 72, 2015. doi:10.3389/fmed.2015.00072.
38. **Westra IM, Mutsaers HA, Luangmonkong T, Hadi M, Oosterhuis D, de Jong KP, Groothuis GM, Olinga P.** Human precision-cut liver slices as a model to test antifibrotic drugs in the early onset of liver fibrosis. *Toxicol In Vitro* 35: 77–85, 2016. doi:10.1016/j.tiv.2016.05.012.
39. **Westra IM, Oosterhuis D, Groothuis GM, Olinga P.** Precision-cut liver slices as a model for the early onset of liver fibrosis to test antifibrotic drugs. *Toxicol Appl Pharmacol* 274: 328–338, 2014. doi:10.1016/j.taap.2013.11.017.
40. **Wollin L, Maillet I, Quesniaux V, Holweg A, Ryffel B.** Antifibrotic and anti-inflammatory activity of the tyrosine kinase inhibitor nintedanib in experimental models of lung fibrosis. *J Pharmacol Exp Ther* 349: 209–220, 2014. doi:10.1124/jpet.113.208223.
41. **Wollin L, Wex E, Pautsch A, Schnapp G, Hostettler KE, Stowasser S, Kolb M.** Mode of action of nintedanib in the treatment of idiopathic pulmonary fibrosis. *Eur Respir J* 45: 1434–1445, 2015. doi:10.1183/09031936.00174914.
43. **Zhang S, Liu Q, Xiao J, Lei J, Liu Y, Xu H, Hong Z.** Molecular validation of the precision-cut kidney slice (PCKS) model of renal fibrosis through assessment of TGF-β1-induced Smad and p38/ERK signaling. *Int Immunopharmacol* 34: 32–36, 2016. doi:10.1016/j.intimp.2016.01.026.
44. **Zhuang S, Liu N.** EGFR signaling in renal fibrosis. *Kidney Int Suppl* 4: 70–74, 2014. doi:10.1038/kisup.2014.13.